Geothermie Delft: Seismic Hazard Analysis

Project: 2200088

October 2022

Geothermie Delft: Seismic Hazard Analysis

Authors

[redacted]

Reviewed by

[redacted]

Release authorised by:

[redacted]

Prepared for

Aardyn
Laan van Barcelona 800
3317 DD Dordrecht
Nederland

Prepared by

PanTerra Geoconsultants B.V.
Weversbaan 1-3
2352 BZ Leiderdorp
The Netherlands
T +31 (0)71 581 35 05
F +31 (0)71 301 08 02
info@panterra.nl

1 Nederlandse samenvatting

Dit rapport geeft een level-2 (locatie-specifieke) Seismic Hazard Assessment (SHA) voor het Geothermie Delft (GTD) project. De score van de GTD SHA level-1 Quick-Scan (Q-CON/IF technology, 2016) werd eerder vastgesteld op 0,3. Deze score betekent dat er een laag seismisch risico is. Om de risico's grondiger te analyseren is een locatie-specifieke SHA uitgevoerd voor de geothermische operatie van GTD.

Figuur 1-1 is een plattegrond van de locatie van de geplande putten DEL GT-01 (productieput) en DEL GT-02 (injector) met naburige breuken. De locatie van de dichtstbijzijnde breuk bij injector DEL-GT-02 is onzeker. Een herinterpretatie door TNO resulteert in een mogelijk kortere minimale afstand tussen injector en breuk (100 m) dan eerder was aangenomen op basis van een interpretatie door PanTerra (400 m).

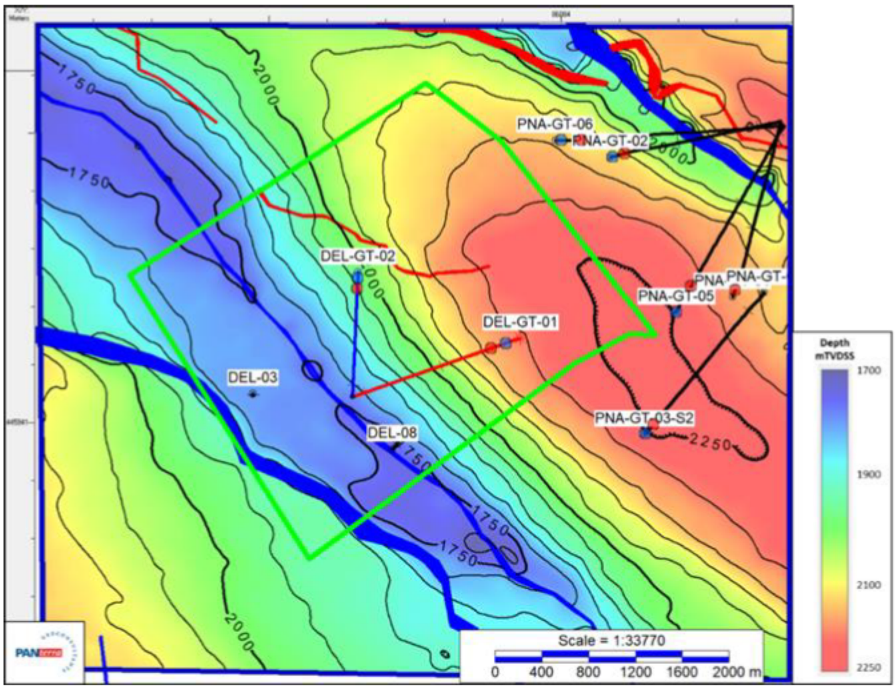

Figuur 1-1 Locatie van de geplande putten DEL GT-01 (productieput) en DEL GT-02 (injector) met naburige breuken.

Geothermie Delft heeft als doel om warm water te produceren uit de Delft zandsteen formatie en om het afgekoelde water met een laagst mogelijke temperatuur van 20°C terug in hetzelfde reservoir te injecteren. Wanneer het geïnjecteerde water een breuk bereikt kunnen de spanningen op die breuk veranderen en in theorie leiden tot breuk reactivatie. Of een breuk mogelijk wordt geactiveerd of niet kan berekend worden door middel van een geomechanische analyse.

Het risico op breukactivatie kan worden uitgedrukt in de parameter SCU (Shear Capacity Utilisation). De SCU is een maat voor de afstand tussen de spanningstoestand waarbij reactivatie optreedt en de berekende spanningstoestand op de breuk. Bij een SCU kleiner dan 1 is breukactivatie onwaarschijnlijk. Zodra deze parameter groter wordt dan 1 bestaat een kans op breukactivatie. Echter bij een SCU>1 hoeft in de praktijk geen breukactivatie op te treden. Bovendien hoeft breukactivatie nog niet te leiden tot seismische activiteit. Op dit moment zijn er in Nederland nog geen geothermische projecten in de operatiefase met een SCU>1 waarbij breukactivatie is waargenomen.

Een relevant fenomeen in deze studie is “arching” (brugvorming) – wat betekent dat niet-afgekoelde delen van het reservoir het gewicht van ondiepere lagen dragen. Dit effect is het sterkst wanneer de laterale extensie van het afgekoelde gebied beperkt is. “Arching” beperkt de kans op breuk reactivatie en het effect hiervan wordt berekend in de geomechanische modellen. Het effect van “arching” kan afnemen gedurende de levensduur van het doublet. Dit komt omdat de laterale extensie van de afgekoelde zone toeneemt naarmate er langer geïnjecteerd wordt. Hoe groter deze laterale extensie wordt, hoe minder “arching” plaatsvindt door aangrenzende niet afgekoelde reservoir zones.

De hier toegepaste workflow is recentelijk ontwikkeld door PanTerra (van den Hoek & Poessé, 2021). Deze workflow is een door Panterra gekozen invulling van een “niveau 2” SHA omdat over deze invulling nog geen officiële richtlijnen bestaan. De werkwijze bevat een reservoirsimulatie van de temperatuurverdeling van het koelere waterfront, en van de thermo-mechanische effecten als gevolg van deze afkoeling, gedurende de periode van een geothermische operatie.

Voor dit doel zijn twee types van geomechanische modellen gebruikt:

1. Een 2-D semi-analytisch model dat het mechanisme weergeeft van mogelijke breukreactivatie door berekening van lokale spanningsveranderingen rond een breuk als gevolg van geothermische operaties gedurende de termijn van de geothermische operatie.

2. Een vertaling van het gereactiveerde deel van de breuk in een magnitude.

De conclusie van deze studie is dat voor 3 jaar water (20°C) injectie in de Delft formatie, onder zeer conservatieve aannamen, de maximale mogelijke magnitude van een eventuele beving gelijk is aan 2.5 bij een afstand van 100 m tussen de injector en de breuk. Bij een afstand van 250 m is de maximale mogelijke sterkte gelijk aan 2.3. Bij een afstand van 400m is de stabiliteit van de breuk vrijwel gelijk aan de stabiliteit voor aanvang van injectie en kan er geen reactivatie optreden. Na 35 jaar operatie is de breuk vrijwel geheel afgekoeld tot de injectietemperatuur van 20°C. In dit geval is de maximale mogelijke sterkte van een eventuele beving gelijk aan 3.1.

Tot op heden zijn geen seismische gebeurtenissen of aardbevingen als gevolg van geothermische operaties gerapporteerd in Nederland. Mocht in de toekomst seismische activiteit als gevolg van geothermische operaties geregistreerd worden door seismische sensoren, dan zullen de gebruikte modellen worden gekalibreerd en de voorspellingen worden bijgesteld.

Contents

2 Introduction

2.1 Area of interest

The Geothermie Delft (GTD) doublet is situated in the municipality of Delft in the province Zuid-Holland. The doublet consists of producer DEL-GT-01 and injector DEL-GT-02 (Figure 2-1). The target reservoirs are the fluvial sands of the Delft Sandstone Member, which is the main target of other doublets in this region.

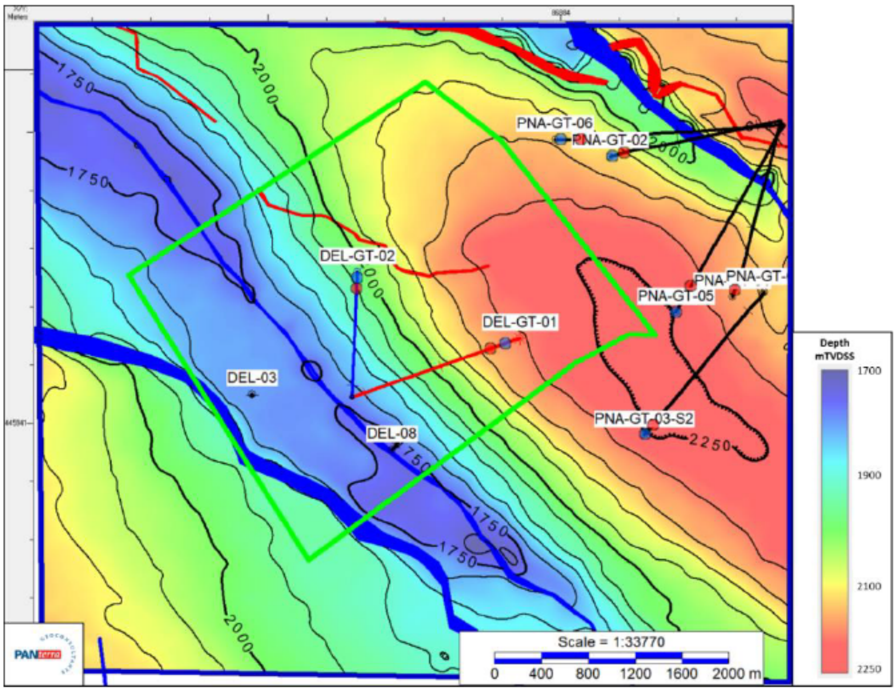

Figure 2-1 Location of planned wells DEL GT-01 and DEL GT-02 with neighbouring faults.

As Figure 2-1 shows, a fault was mapped by PanTerra at ~400 m from the injector. This fault was reinterpreted by TNO at a closest distance of 100 m from the injector.

2.2 Guidelines for geothermal projects

A decision tree (Figure 2-2) for carrying out a Seismic Hazard Assessment (SHA) has been made by QCon/IF technology (2016). This decision tree contains three risk levels, with required levels of relevant studies associated to it. A Level 1 SHA (lowest level 'QuickScan') was carried out for GTD as part of the production license application. The resulting score from the SHA QuickScan was determined to be equal to 27/90 for the planned GTD doublet (Figure 2-3). This is associated with low seismic risk. However, if the pre-drill SHA QuickScan is filled out in a more conservative manner, since some parameters are theoretically unknow pre-drill, the resulting score might touch Level 2, and a location specific seismic hazard analysis shall be performed.

Therefore, to demonstrate prudence, an independent detailed geomechanical study (location-specific seismic hazard assessment) was performed for the geothermal operation of GTD. This report touches upon the aspects that are involved in a Level 2 SHA. The current guidelines by QCon/IF only partially define the Level 2 SHA and no clear framework exist for how to conduct such a study. For this reason a recently developed new SHA-methodology (van den Hoek & Poessé, 2021) was applied for GTD.

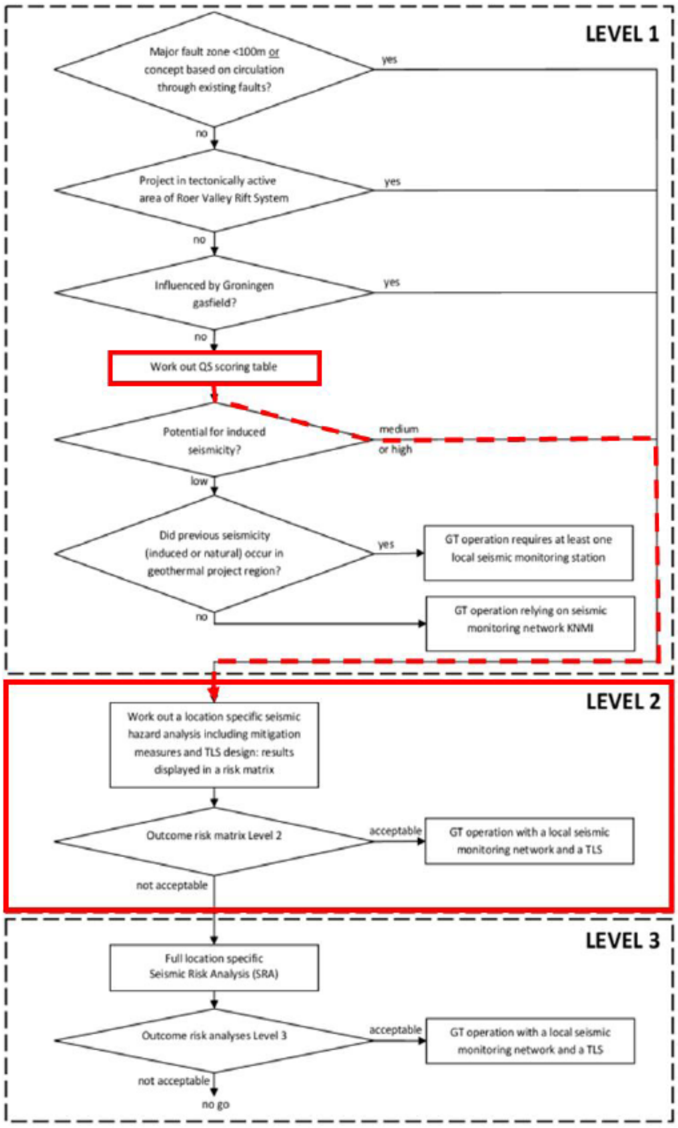

Figure 2-2 Decision tree as presented in the report by Q-CON/IF technology (2016). In this report Level 2 (red outline) is covered. TLS stands for Traffic Light System.

Score	Basement connected	Inter-well pressure communication	Re-injection pressure [MPa]	Flow rate [m³/h]	Epicentral distance to natural earth quakes [km]	Epicentral distance to induced seismicity [km]	Distance to fault [km]	Orientation of fault in current stress field	Net injected volume [1000 m³]
10	Yes	No	>7	>360	<1	<1	<0.1	**Favourabl e**	>20
7	Possible	Unlikely	4-7	**180-360**	1-5	1-5	**0.1-0.5**	Shearing possible	5-20
3	Unlikely	Likely	**1-4**	50-180	5-10	5-10	0.5-1.5	Shearing unlikely	0.1-5
0	**No**	**Yes**	<1	<50	**>10**	**>10**	>1.5	locked	**<0.1**

Figure 2-3 Seismic Hazard Assessment QuickScan for the GTD project.

3 Methodology

Because currently no guidelines exist for carrying out a Level 2 Seismic Hazard Assessment (SHA), the methodology used in this study is based on the recently proposed approach by van den Hoek & Poessé (2021). Geo-mechanical models were created to understand the thermo-mechanical effects in the lifetime of the GTD geothermal operation. Van den Hoek & Poessé (2021) used a semi-analytical analysis to carry out a detailed study of the stress changes along nearby faults as a result of geothermal operations over the lifetime of a field. In the current study, the same approach is used. The semi-analytical model can be considered as an exact solution to the stress concentrations induced by cooling. The focus of this study is the geomechanical effects in the Delft formation. The approach to simulate the stress changes induced by cooling is presented in some more detail in section 3.1 below. The 2-D Mohr-Coulomb model uses a deterministic methodology and an uncertainty analysis. The uncertainty analysis was presented in 2020 by Poessé & van den Hoek (2020) and is summarised in section 3.2.

Until now, no seismic events or small earthquakes have been reported in The Netherlands as a result of geothermal operations (https://kennisbank.ebn.nl/reviewstudie-seismiciteit-tno/). In the future, if seismic sensors would detect seismic activity resulting from geothermal operations, the models can be calibrated and predictions could be updated.

3.1 Two-dimensional semi- analytical model to simulate stress changes induced by cooling

The semi-analytical model is based on an elaboration of the so-called Goodier integral expression for stresses induced by changes in reservoir pressure and / or temperature, see for example Koning (1988). This results in an exact solution of the induced stress changes, and therefore comparison with finite element calculations of the same geometry should give good agreement. This agreement was achieved in a validation study by PanTerra that was carried out as part of the in-house model development.

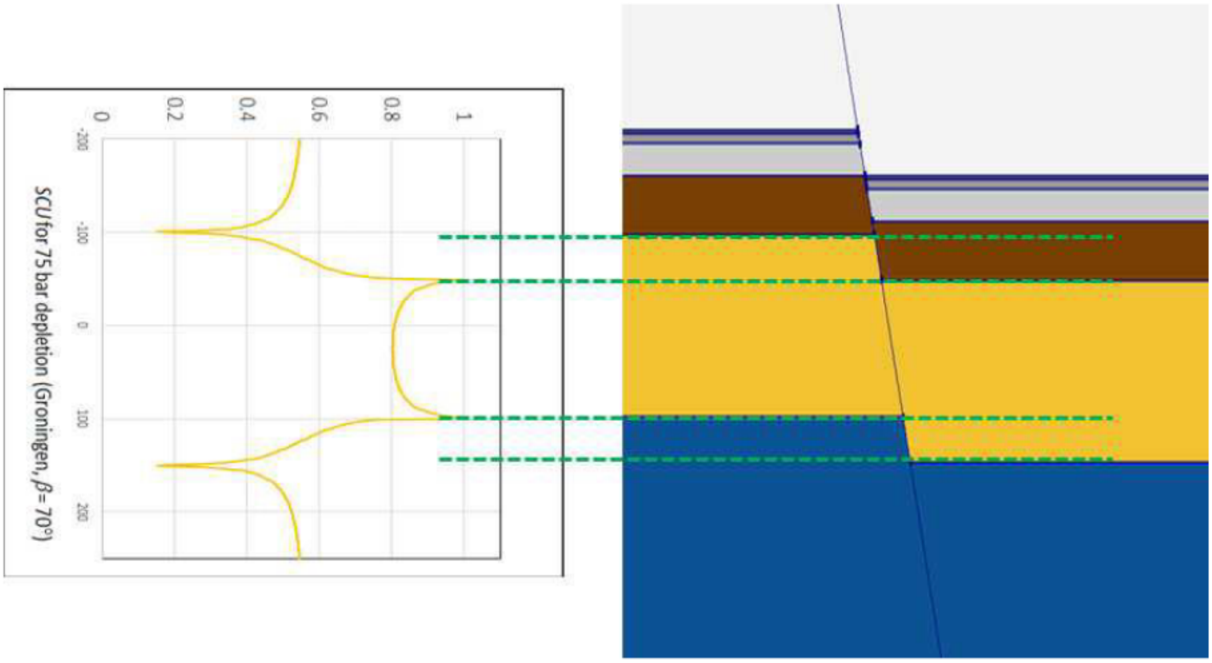

Figure 3-1 Profile of the computed "Shear Capacity Utilisation" (SCU) along the fault for a field situation, with 75 bar reservoir depletion (e.g. due to gas-production).

Figure 3-1 shows a typical result as computed for the example of 75 bar depletion in the field (e.g. due to gas-production). The case of stress concentrations on the fault as a result of reservoir depletion has been widely published, see for example Buijze et al. (2017), Poessé & van den Hoek (2020), van den Hoek and Poessé (2021), and van den Bogert (2015). Figure 3-1 shows the profile of the so-called “Shear Capacity Utilisation” (SCU) along the fault which is defined by

$$SCU = \div \frac{\text{Shear stress along the fault}}{\text{Maximum shear stress along the fault}} = \frac{\text{Shear stress along the fault}}{C + (\text{Normal stress on the fault}) \times \tan(\varphi)}$$

where C and φ are the cohesion and friction angle of the fault, respectively. The SCU can be viewed as a quantitative measure of how close the fault is to “failure” (activation), which is indicated by a value of SCU = 1. In Figure 3-1 it can be seen that there are shear stress concentrations, resulting in high SCU, at the top of the hanging wall reservoir (right) and the bottom of the foot wall reservoir (left). This is a well-known phenomenon that takes place along faults with nonzero offsets crossing depleting reservoirs, see again van den Bogert (2015), Poessé & van den Hoek (2020), van den Hoek & Poessé (2021), and TNO (2014). With progressing reservoir depletion beyond 75 bar, the SCU of the entire fault area between the top of the hanging wall (right) and bottom of the foot wall (left) becomes equal to one, which eventually could cause fault slip over this area. This potential movement along the fault does not directly imply that seismicity and small earthquakes will occur (Poessé & van den Hoek, 2020), (van den Hoek & Poessé, 2021). The methodology can only calculate the possible reactivation of a fault but not whether that will happen seismically or a-seismically. One other (non-realistic) assumption in the model is the uniform distribution of the strength parameters of the fault.

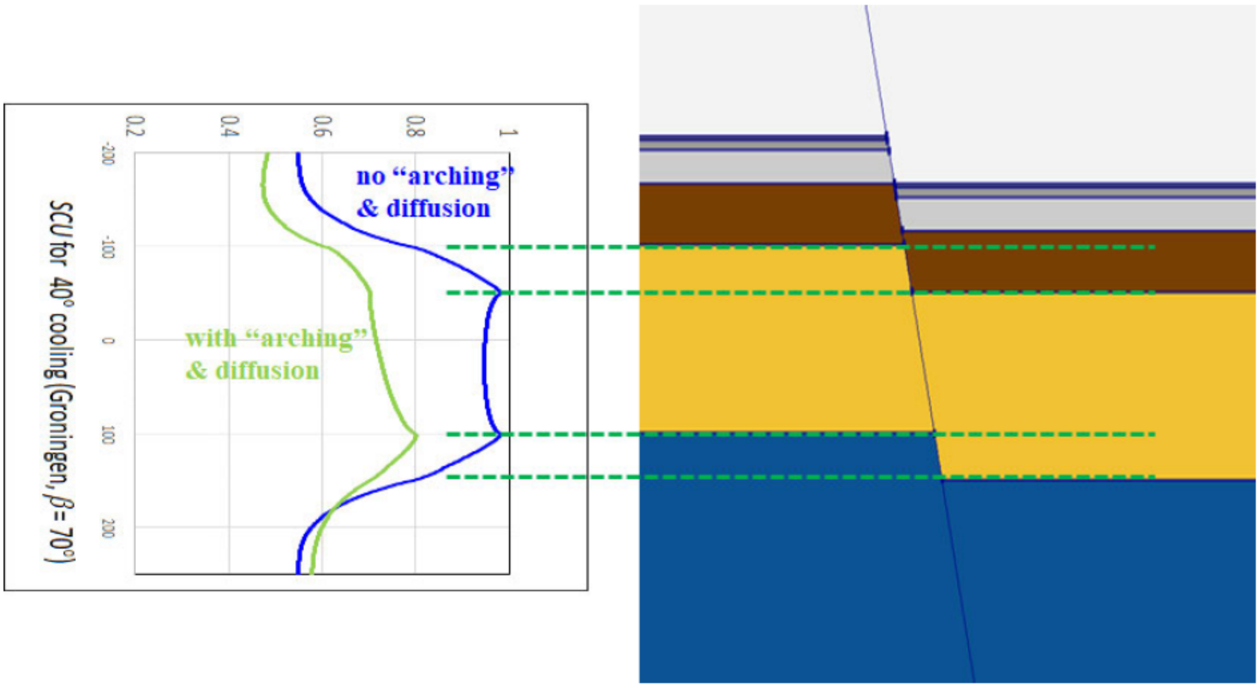

Figure 3-2 Profile of the computed “Shear Capacity Utilisation” (SCU) along the fault for a field situation, with (hypothetical) 40°C reservoir cooling.

The effect of stress concentration along faults with nonzero offsets not only takes place as a result of reservoir depletion, but also as a result of reservoir cooling. Stress changes, as an effect of reservoir cooling, are illustrated in Figure 3-2 for the same reservoir as Figure 3-1, but now for a (hypothetical) cooling by 40°C. However, an essential difference with (gas) reservoir depletion is that in this case, only a very limited part of the reservoir is cooled, even after around 30 years of operation. Moreover, as a result of thermal diffusion within the reservoir and from the cap- and base-rock, the temperature varies more smoothly and large parts of the reservoir, especially further away from the injector, cool only partially. The finite size of the (partially) cooled reservoir results in arching by the non-cooled areas of the reservoir, and therefore the SCU at the fault can be significantly lower. This is illustrated in Figure 3-2. Here, the blue curve represents a situation where the entire reservoir has been cooled, whereas the green curve represents a situation where only a few hundred meters around the injector have been (partially) cooled.

3.2 Mohr-Coulomb modelling

The state of stress can be defined by the means the Mohr-circles and associated Mohr-Coulomb failure criterion. The Mohr-circle represents the state of stress for any given orientation in a 2D or 3D space, with as input the maximum, minimum and in case of 3D the intermediate stress. In the presence of a fault, a failure criterion can be defined by the cohesion and friction coefficient of this fault. If the state of stress in a specific orientation exceeds the failure criterion, shear slip movement may occur along the fault. The goal of the Mohr-Coulomb exercise is to know at what condition slip along the fault may occur which is a potential hazard coming from a subsurface operation.

Mohr-Coulomb only addresses the stress state at one point in space. In order to address parameter uncertainties, an uncertainty Mohr-Coulomb approach is applied to the point along the fault where failure is most likely, i.e. the point with highest SCU. This can be considered a conservative approach because it only addresses the failure likelihood of *the "worst" point along the fault*, whereas fault slip requires failure (SCU = 1) over a larger continuous fault area, just like in the depletion case.

In a uncertainty Mohr-Coulomb study, 1000 simulations are run on a large range of parameters covering the state of stress, production parameters, geological and rock parameters, fault parameters and arching and temperature diffusion. A triangular distribution is used to omit outliers as is consistent with the DoubletCalc approach, TNO (2014).

3.3 Temperature profile

The temperature profile is computed by an in-house fine-grid radial numerical reservoir simulation. An example is shown in Figure 3-3, which shows that this model predicts a more conservative (= larger) cold front radius than DoubletCalc2D. For reference, also the radius based on an analytical heat balance calculation is included. In the absence of thermal diffusion from cap- and base-rock, the numerically computed centre of the cold front should coincide with this line.

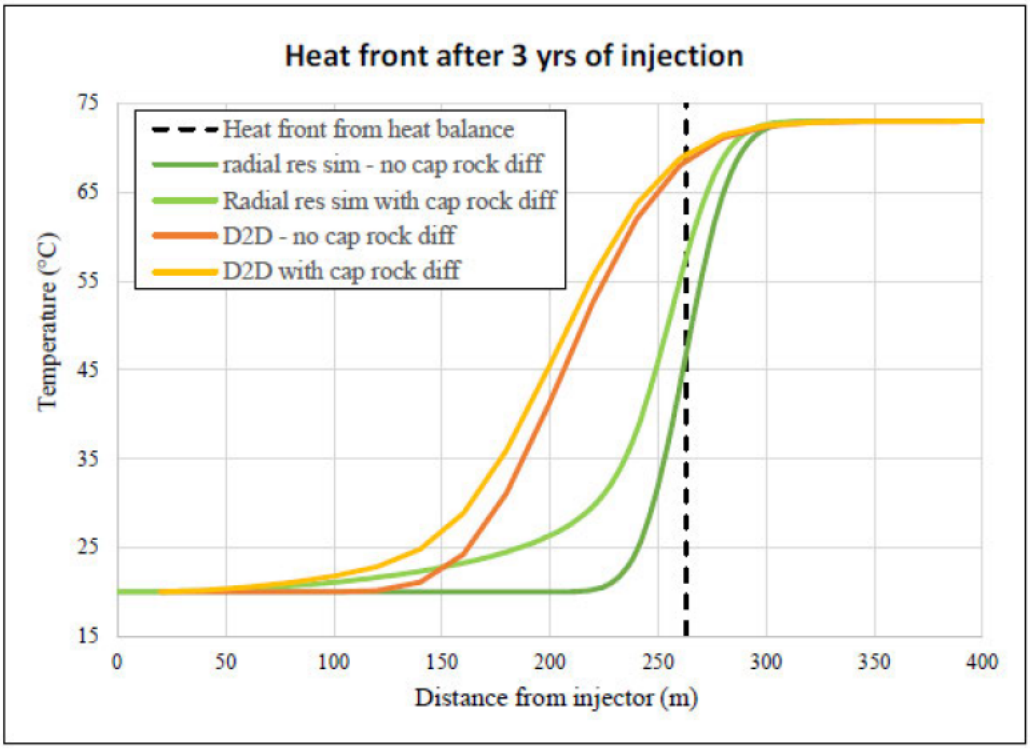

Figure 3-3 Temperature profiles as computed by our model and by DoubletCalc2D, both without and with thermal diffusion from cap- and base-rock. Dashed line represents the position of the heat front based on analytical heat balance calculation. In the absence of thermal diffusion from cap- and base-rock, the centre of the cold front should coincide with this line.

4 Geological and geomechanical setting

4.1 Geological setting

The GTD doublet will be situated in the West Netherlands Basin (WNB, Figure 4-1), which is an inverted rift basin (de Jager et al., 1996). Sediments in this basin range in age from Jurassic to recent and are overlying Triassic and older sediments. The reservoir targets is the Cretaceous Delft Sandstone Member. The Delft Sandstone has good reservoir properties in general.

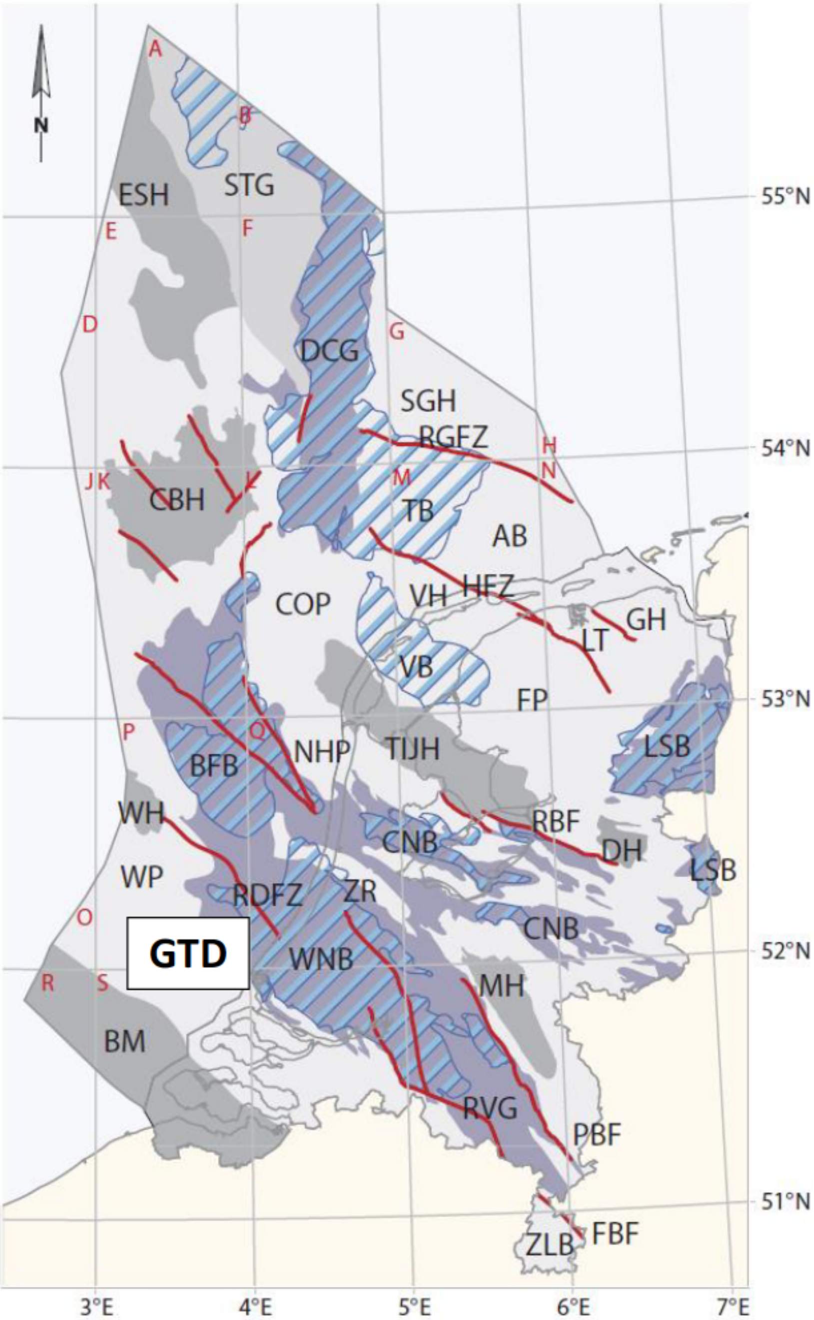

Figure 4-1 Structural elements and major fault zones as present during the Late Jurassic-Early Cretaceous (Duin et al., 2006).

In the Late Cretaceous, during the deposition of the Chalk Group, the West Netherlands Basin was inverted. This was accompanied by compressional movements and resulted in convergent oblique-slip faulting, general uplift, erosion and basin inversion, which reactivated pre-existing normal faults. The major tectonic feature in the region of the license is a NW-SE trending half graben. The structure is bounded by a number of faults.

At reservoir level, injector DEL-GT-02 is located approximately 400 m away from a small tapering fault (indicated in red in Figure 4-2). There is some uncertainty on the exact location of this fault, which can lead to different closest distances between injector DEL GT-02 and the interpreted fault (ranging from 400m to 100m).

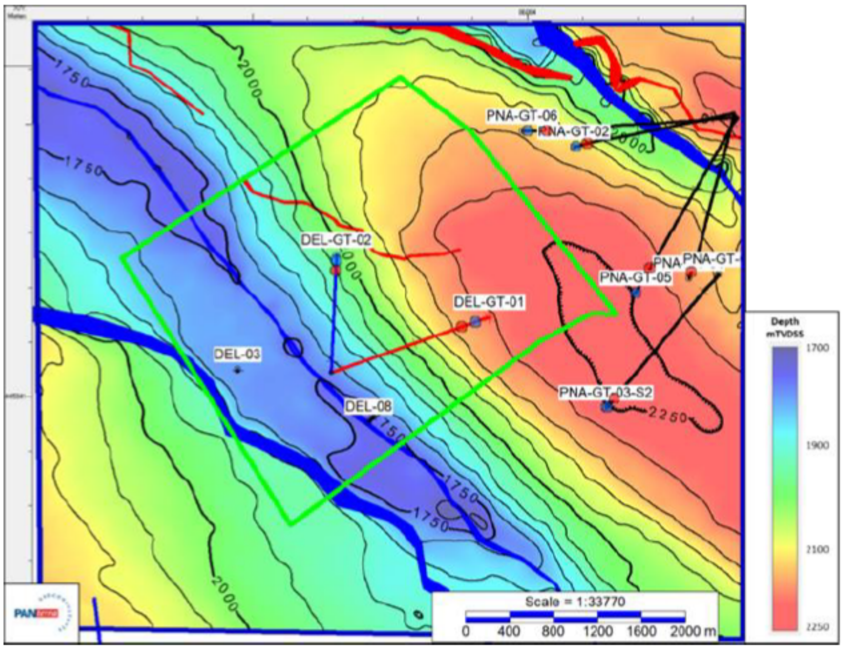

Figure 4-2 Top Delft reservoir depth map of the target area with planned wells, penetration points and faultlines.

The fault in question has a low offset with some uncertainty in it, is vanishing towards the east, and seems to be absent close to the producer. In the current study, we use an upper limit to the fault offset of 25 m, as this is the most conservative estimate. Figure 4-3 provides a schematical overview of the fault as used in the current study.

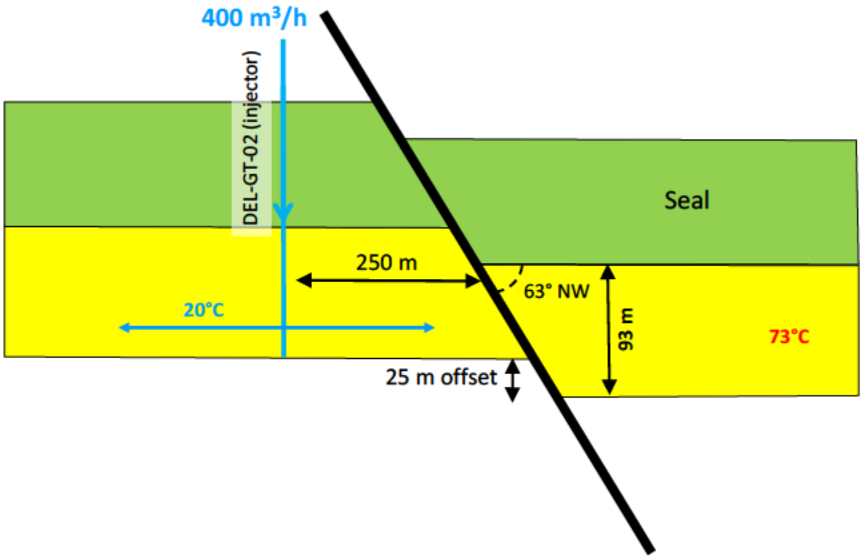

Figure 4-3 Fault and geometrical information for injection well DEL-GT-02. In this study the distance between the injector and the fault ranges between 100-250-400m.

4.2 In-situ stress estimates

In-situ stress trends are mostly based on measured leak-off pressures as reported by Verweij et al. (2012). These authors distinguished a number of different geological areas within the Netherlands. For each of these areas, an in-situ stress trend map was generated. The geological area that is relevant for the current discussion is the so-called West Netherlands Basin (WNB) for which the data are given in Figure . This figure displays measured leak-off pressure tests (LOT) as a function of depth in the West Netherlands platform area. This figure is based on those tests in the NLOG database that have been clearly marked 'LOT', i.e. all non-LOT and tests where there is possible doubt have been left out.

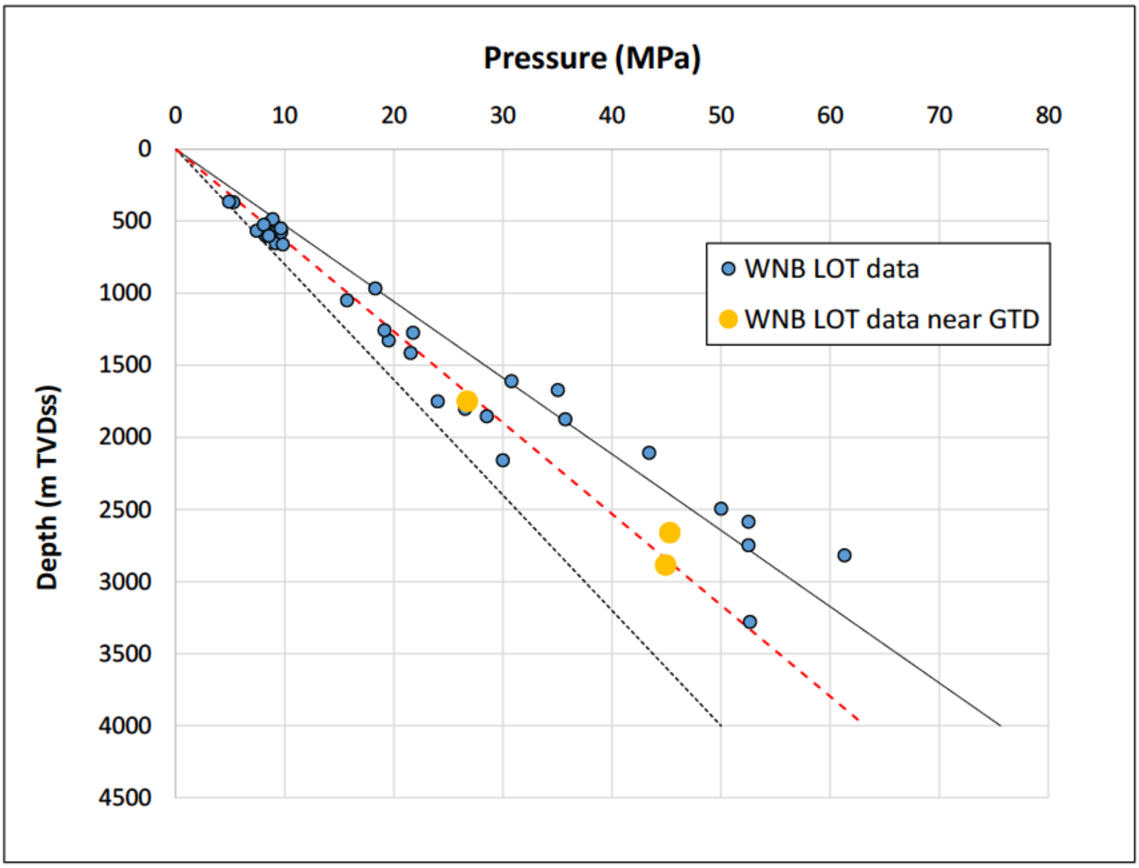

Figure 4-4 Minimum in-situ stress versus depth trend in the West Netherlands Basin area based on Leak-Off Tests (NLOG database). Red-dashed line: trend line based on leak-off tests.

From the dataset shown in Figure , a subset was chosen from wells in the neighborhood of Delft. The wells chosen for this subset are displayed in Figure . The subset is shown by the yellow dots in Figure 4-4. As can be seen, the baseline trend falls more or less on top of the well-known trend of 0.158 bar/m for an extensional stress regime. The lower bound is given by 0.125 bar/m based on minifrac test results in the The Lier sandstone in the Rotterdam field.

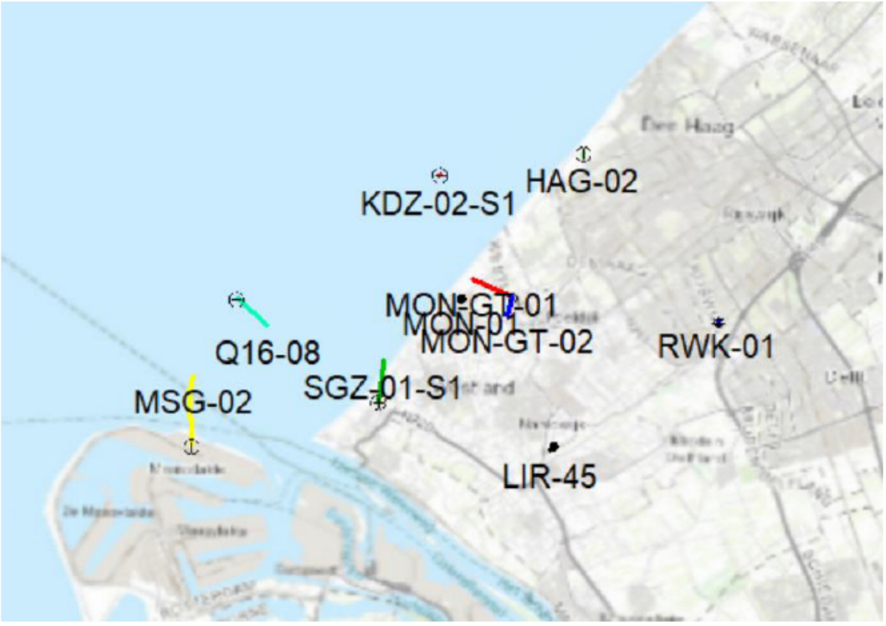

Figure 4-5 Wells in the neighborhood of GTD for subset of LOT data.

4.3 Reservoir Parameters

Reservoir parameters have an influence on both the production prognosis as the geomechanical calculation and will be shortly discussed below.

4.3.1 Depth

Top of the reservoir near the injector well is reported at 1957 m TVD for the Delft.

4.3.2 Thickness

The median thickness of the Delft is estimated to be 93 m near the injector well.

4.3.3 Temperature

Based on data from DoubletCalc, reservoirs temperature near the injector well has been set to 73°C.

4.3.4 Thermo-elastic constant

In response to temperature changes, the reservoir rock will tend to expand (heating) or shrink (cooling). Because in the subsurface there is no 'room' in the horizontal direction to expand or shrink ('plane strain'), this results in a change of total horizontal stress that is given by

$$\Delta\sigma_{\mathrm{h}} = A_{\mathrm{T}}.\Delta T \qquad (4.1)$$

where ΔT is the temperature change (negative for cooling) and A_T is the "thermo-elastic constant" (in bar/°C). Equation (4.1) is only valid if the entire reservoir has been cooled. When only part of the reservoir has been cooled, a geometry correction factor is applied. This geometry correction factor is also included in our semi-analytical model.

The thermo-elastic constant is a material property of the rock. Under the assumption of perfectly elastic behaviour of the rock, both at matrix level and at grain level, this constant can be expressed as

$$A_{\mathrm{T}} = \frac{\alpha E}{1-\nu} \qquad (4.2)$$

where

- α is the linear thermal expansion coefficient (in °C^{-1})
- E is Young's modulus (in bar)
- ν is Poisson's ratio (dimensionless)

suggesting that A_T is linearly proportional to Young's modulus E if the thermal expansion coefficient α is assumed equal for all types of rocks under all circumstances (stress, temperature).

Not many measurements of the thermo-elastic constant have been carried out. Koning (1988) and Perkins & Gonzalez (1985) used values for A_T in the range 0.9-1.0 bar/°C for 'medium-strength' reservoir sandstones with Young's moduli in the range 10-15 GPa. For deep, tight rocks (> 10000 ft TVD), values of A_T in the range 1.5-2.0 bar/°C have been used in a number of oil field studies with waterflooding, both in Prudhoe Bay, Alaska (Stevens et al., 2000) and in the North Sea (Santarelli et al., 2008; Svendsen et al., 1991). On the other hand, in the Eider oil field, North Sea (~ 9000 ft TVss) a value of A_T = 0.6 bar/°C was derived based on step-rate tests, whilst in a carbonate / mudstone reservoir in the Middle East (~6500 ft tVD), a range of 0.4-0.9 bar/°C was measured on different core plugs. From the above we derive an average value for A_T of ~1.0 ± 0.5 bar/°C, which may increase up to ~ 2,0 bar/°C for (very) tight rocks. In the current study a value of 1.0 ± 0.5 bar/°C is used

4.3.5 Poro-elastic constant

In response to pressure changes, the reservoir rock will tend to expand (pressurisation) or shrink (depletion). Because in the subsurface there is no 'room' in the horizontal direction to expand or shrink ('plane strain'), this results in a change of total horizontal stress that is given by

$$\Delta\sigma_{\mathrm{h}} = A_{\mathrm{p}}.\Delta p \qquad (4.3)$$

where Δp is the pressure change (negative for depletion) and A_p is the "poro-elastic constant" (dimensionless). Equation (4.3) is only valid if the entire reservoir has been pressurised or depleted. When only part of the reservoir has been pressurised / depleted, a geometry correction factor is applied. This geometry correction factor is also included in our model.

The poro-elastic constant is a material property of the rock. Under the assumption of perfectly elastic behaviour of the rock, both at matrix level and at grain level, this constant can be expressed as

$$A_{\mathrm{p}} = (1-\beta)\frac{1-2\nu}{1-\nu} \qquad (4.4)$$

where

- $\beta = \frac{K_m}{K_s}$
- K_{m} is the bulk modulus of the rock matrix (bar)
- K_{s} is the bulk modulus of the solid rock grains (bar)

In practice, the above equation is only of qualitative value. Laboratory tests have shown that A_p often deviates significantly from the formula (4.4). Typical values are in the range 0.5-0.8. In the current study a value of 0.6 is used. Contrary to the thermo-elastic constant A_T, the value used for A_p is less critical because in a typical geothermal doublet, only a very small area around the injector is pressurised and only a small area around the producer is "depleted". On the other hand, a significant area around the injector will be cooled during the field life, thus making the parameter A_T a more critical one.

4.3.6 Fault parameters

Fault stability is defined by the cohesion and friction coefficient of the fault.

4.3.6.1 Cohesion

As a conservative low base, zero cohesion is assumed. For the probabilistic analysis a range of 0-15-30 bar is considered. A cohesion of 15 bar can be considered as 'typical' for weakly consolidated rock.

4.3.6.2 Friction coefficient

No measurements on fault properties are available. A typical sandstone has a friction coefficient in the order of ~0.6 (Hunfeld et al., 2017). This value is valid for cemented sandstones such as the Slochteren sandstone. Uncertainty ranges on sandstone are reported between 0.48 and 0.72 (Samuelson & Spiers, 2012). A range of 0.48-0.60-0.72 is used. No hardening and/or softening of the fault is considered in this analysis.

5 Results

Results of the fault stability near injector DEL-GT-02 will be presented for the situation after 3 years of injection and after 35 years of injection.

5.1 Temperature profile after 3 years of injection

The computed temperature profile away from the injector after 3 years of injection is presented in Figure 5-1. The cooled zone is not an abrupt front but rather influenced by thermal diffusion, both within the reservoir and from the cap- and baserock into the reservoir.

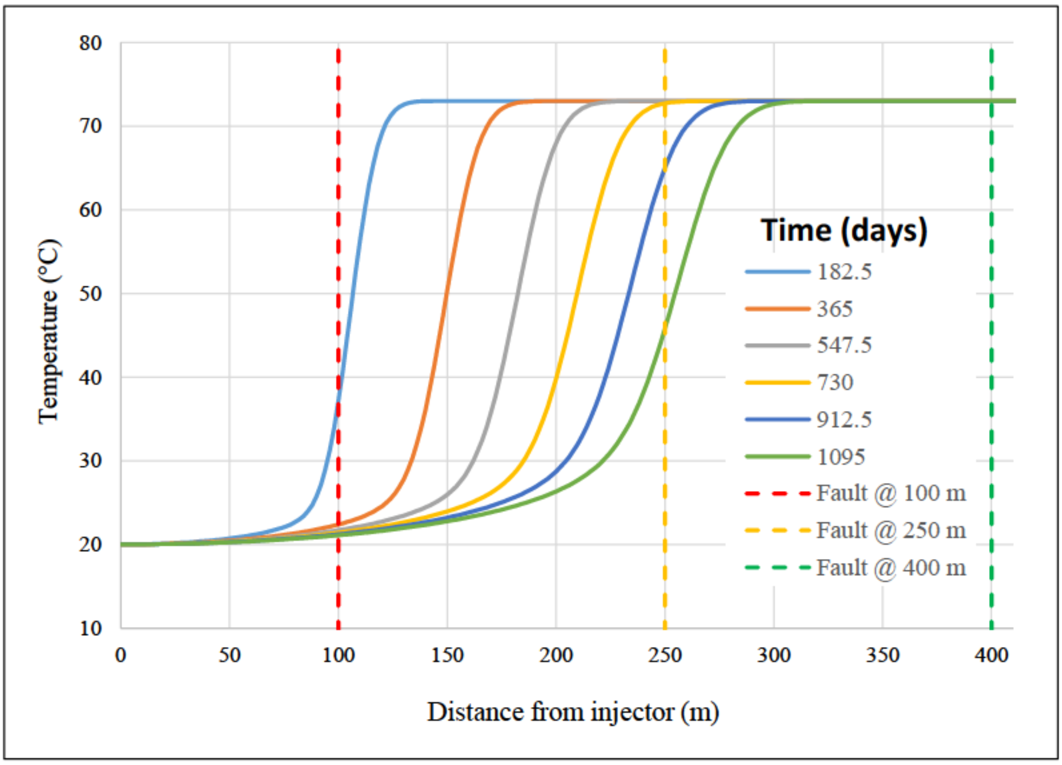

Figure 5-1 Temperature profile in the reservoir away from the injector after 3 years of injection.

After 3 years of injection we observe a temperature alteration up to about 300 m from the injector. This is considered the cold water "front".

The geometry of the situation is sketched in Figure 4-3 above. As mentioned earlier, there is some uncertainty on the exact location of this fault. Different fault mappings lead to different closest distances between injector DEL GT-02 and the fault. In the current study, distances of 100 m, 250 m and 400 m are evaluated. As can be seen from Figure 5-1, the distance between fault and injector has a significant impact on the degree of cooling at the fault after 3 years of injection.

5.2 Deterministic analysis after 3 years of injection

The methodology as described in section 3.1 is applied to estimate the impact of the cooling on the Shear Capacity Utilisation (SCU). In order to take into account the effect of partial cooling, the entire temperature profile in the cooled zones to the left and to the right of the fault is computed. Subsequently, the thermo-elastic stress change on the fault resulting from this temperature profile is calculated.

The results are given in Figure 5- where the SCU is calculated for the initial state (vertical blue line) as well as the state of the fault affected by a nearby cooled area. This shows the computed SCU along the fault after 3 years of injection. As can be seen, the SCU profiles vary significantly depending on the distance between injector DEL-GT-02 and the fault.

For 400 m distance, the SCU has hardly changed with respect to the initial situation. This is not surprising, as in this case the cold front has not yet reached the fault (Figure 5-1). Please note however, that the SCU change with respect to the initial state is not entirely zero, because a thermal stress change in the area to the left of the fault (Figure 5-2) should already have a (modest) impact on the shear stress on the fault itself. This has been adequately captured in our model.

On the other hand, for 100 m distance between injector and fault, the SCU at the fault has changed significantly (Figure 5-2) as a result of (almost) complete cooling (Figure 5-1) of the area around the fault.

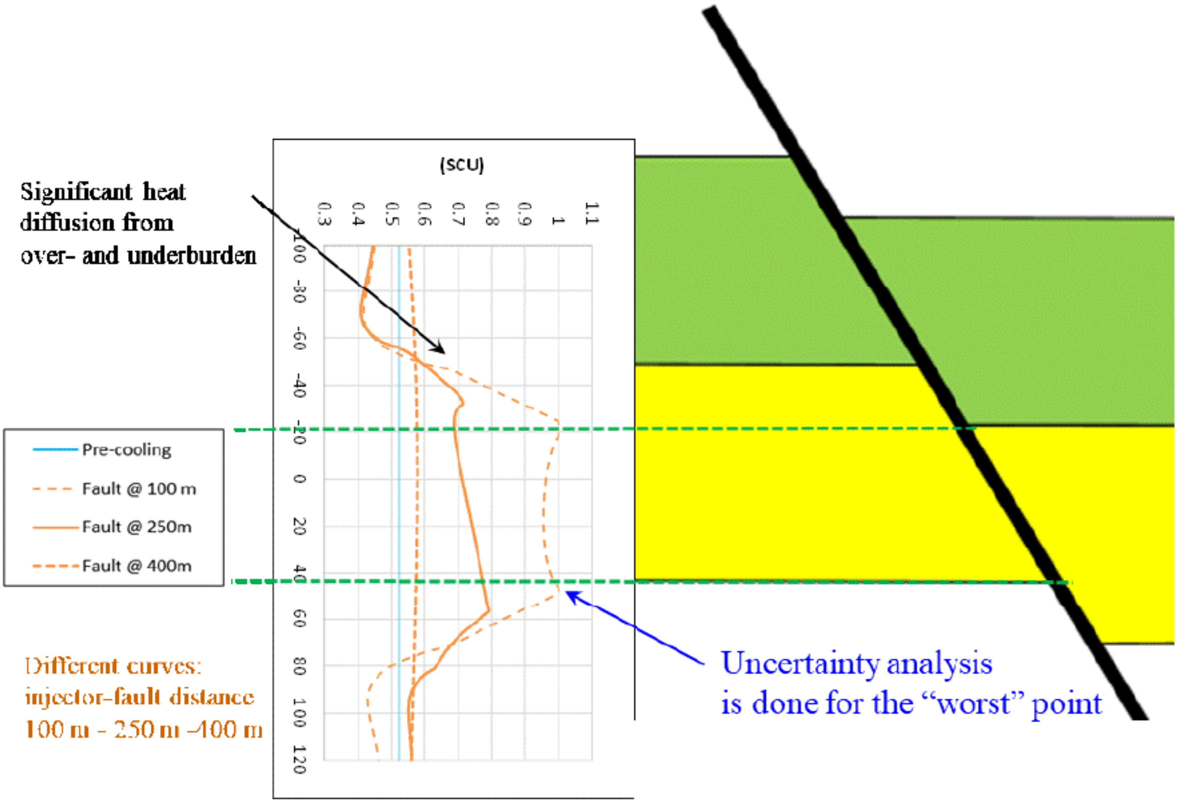

Figure 5-2 Computed SCU along the fault after 3 years of injection. The three different curves indicate the SCU-profiles for a fault at 100 m – 250 m – 400 m.

5.3 Uncertainty analysis

In order to address the impact of parameter uncertainties, an analysis was carried out using an ensemble of 1000 random but realistic parameter-combinations. The addressed parameters are shown in Table 5-, which displays the input parameters for the uncertainty analysis of the Delft formation and the fault, including their low-med-high values. The parameters and reasoning have been discussed in section 4.3.

Table 5-1 input parameters for uncertainty analysis

	Parameter	Low	Medium	High
Rock Parameters	Reservoir Temperature (°C)	71	73	75
	Thermoelastic coefficient (bar/°C)	0.5	1.0	1.5
	Vertical stress gradient (bar/m)	0.21	0.22	0.23
	Horizontal stress gradient (bar/m)	0.125	0.158	0.189
Fault Parameters	Cohesion (bar)	0	15	30
	Friction coefficient (-)	0.48	0.60	0.72
	Dip (degrees)	53	63	73
	Distance from injector (m)	100	250	400

5.4 Fault reactivation energy and seismic magnitude

The uncertainty analysis form the basis of estimating the fault reactivation energy and, from that, the strength (magnitude) of the realistically strongest possible seismic tremor as a result of fault slip. Underlying assumptions of this approach are the following:

- The "magnitude" M_w is estimated from fault reactivation energy
- This "magnitude" is the maximum upper bound for seismic tremors
- It is assumed that the formation rock around the fault behaves in an elastic-brittle manner in response to cooling-induced stress disturbances (→ reactivation energy is released at once)
- In reality, because of the shallow reservoir, most of the rock is expected to behave elasto-plastically in response to cooling-induced stress disturbances (→ reactivation energy is released gradually in small quantities over time)
- No difference in horizontal in-situ stress between reservoir and cap-/baserock assumed
- However, cap- and base-rock are mostly at higher pre-cooling values of minimum horizontal stress than reservoir and therefore less likely to reach SCU > 1 during field life
- The same fault strength is assumed over the entire reservoir and over cap-/baserocks.

Calculation of fault reactivation energy and maximum M_w is based on the methodology as published by Staatstoezicht op de Mijnen (2016). For each of the 1000 random parameter-combinations, the seismic moment M_0 is calculated according to the formula

$$M_0 = \frac{3\pi}{8} \Delta\sigma \, w^2 \, L \tag{5.1}$$

where M_0 is the seismic moment (in Joule), $\Delta\sigma$ is the relaxation stress drop (in Pascal), and w and L are the height and length (in m), respectively, of the (cold front-affected part of) the fault. Please note that the stress drop $\Delta\sigma$ for fault relaxation is only nonzero where the SCU prior to relaxation ≥ 1. The seismic moment M_0 is considered to be a measure of the *maximum* amount of energy that is released when the *entire* fault relaxes at once.

From the seismic moment M_0, the maximum strength (magnitude) M_w of the realistically strongest possible seismic tremor is calculated according to

$$M_w = \frac{2}{3}\left({}^{10}\log M_0 - 9.1\right) \tag{5.2}$$

Using (5.1) and (5.2), for each parameter-combination we go through the following steps:

- Compute the temperature profile using the methodology as presented in chapter 4 above (reservoir simulation)
- From this temperature profile, compute the SCU-profile along the fault using the methodology as presented in chapter 4 above (2D integration of thermo-elastic and/or poro-elastic stress changes)
- Compute w = total height of the fault area where SCU ≥ 1
- Compute $L = 2 \times \sqrt{(Thermal\ front\ radius)^2 - (Distance\ injector - fault)^2}$
- Estimate $\Delta\sigma$ for those areas along the fault where SCU ≥ 1

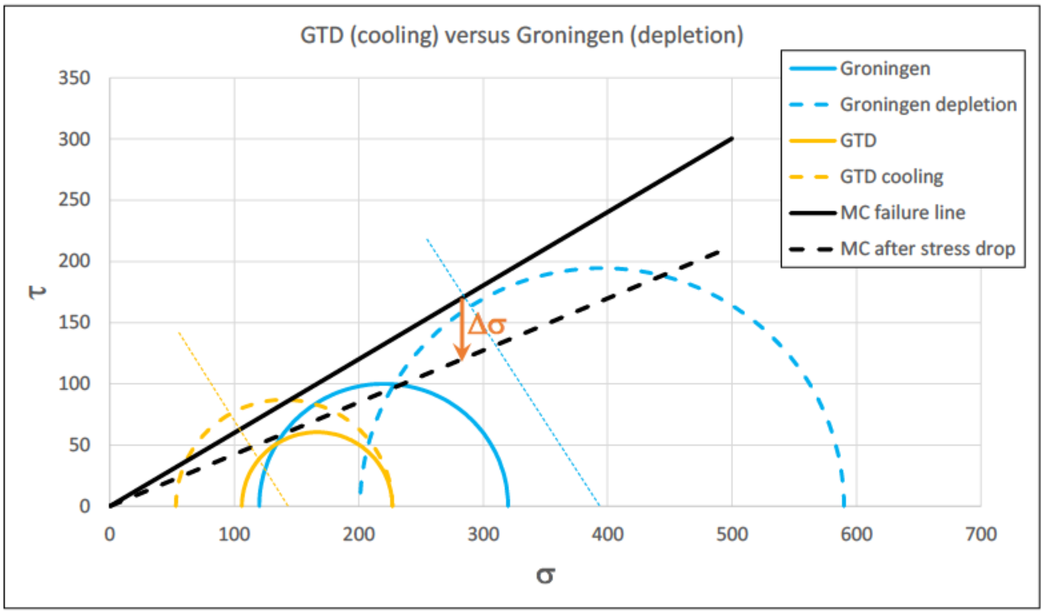

Figure 5-3 Estimation of relaxation stress drop Δσ.

The relaxation stress drop Δσ is estimated using a "semi-empirical" method, see Figure 5.3. Upon fault reactivation (reaching the Mohr-Coulomb failure line, solid line in Figure 5-3) relaxation will cause a reduction in the friction angle φ resulting in a new Mohr-Coulomb failure line (dashed line in Figure 5-3). This in turn causes a stress drop Δσ. For most induced earth quakes, the observed stress drop Δσ does not exceed 50 bar (SodM, 2016). This has been indicated in Figure 5-3. The "semi-empirical" method consists of estimating a reduction Δφ of the friction angle such that this results in a stress drop of 50 bar for Groningen. For an initial value of φ = 31° (corresponding to a friction factor of 0.6, see Table 5-1) this corresponds to a drop Δφ of 8°. As can be seen, such a drop in φ will cause a stress drop in GTD in the order of 50/3 ≈ 17 bar. As is also shown in Figure 5-3, the precise value of this stress drop will be proportional to the effective normal stress on the fault at the moment of reactivation.

5.5 Uncertainty analysis and maximum M_w after 3 years of injection

5.5.1. Fault-injector distance 100 m

For each set of parameter-combinations, it is necessary to estimate which part of the fault is subjected to SCU ≥ 1 after three years of injection and injector-fault distance of 100 m. This is done via the "proxy"-parameter of maximum SCU, see Figure 5-4.

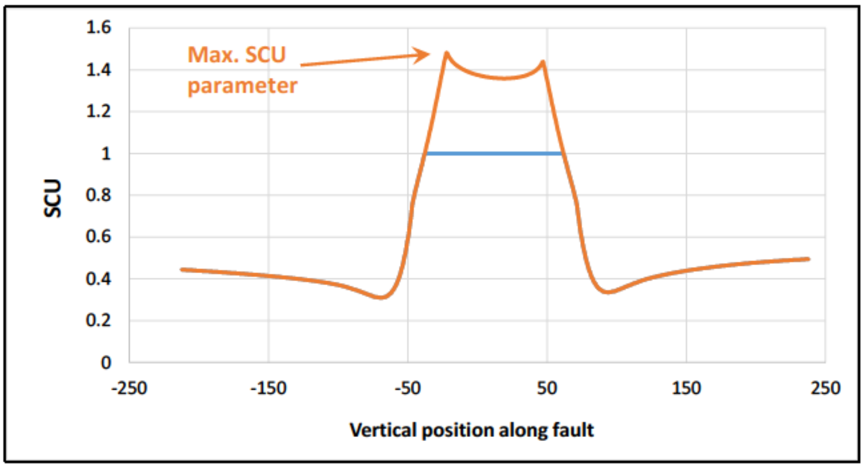

Figure 5-4 Example of SCU-profile along the fault, indicating which part of the fault is subjected to SCU ≥ 1, after three years of injection and injector-fault distance of 100 m.

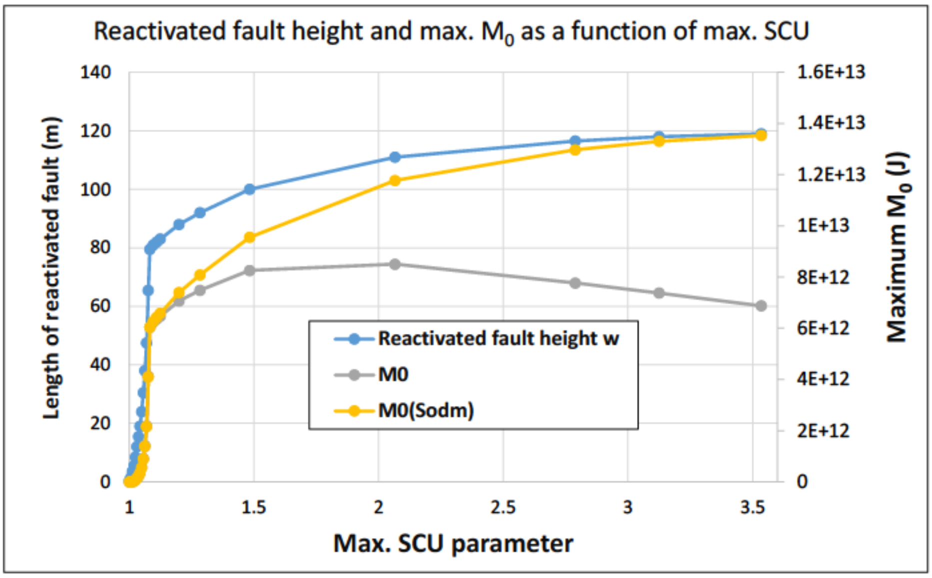

Figure 5-5 Reactivated fault height w and maximum seismic moment M_0 as a function of maximum SCU, after three years of injection and injector-fault distance of 100 m.

Figure 5-5 shows the reactivated fault height w and seismic moment M_0 as a function of maximum SCU. The curve labeled "M_0" depicts the M_0 as computed using equation (5.1), whilst the curve "M_0(Sodm)" also depicts the M_0 as computed using equation (5.1) but then with a fixed value of Δσ equal to 17 bar. As can be seen from Figure 5-5, the higher this value of maximum SCU, the higher is the reactivated part of the fault.

As can be seen, initially (for SCU hardly exceeding one), the reactivated fault height increases rapidly as a function of maximum SCU. This corresponds to the maximum SCU-range where the two peaks and valley in between of the SCU-profile (see Figure 5-4) start to exceed one. A zoom-in of the results of Figure 5-5 on maximum SCU-range between 1 and 1.14 is depicted in Figure 5-6, clearly illustrating this point.

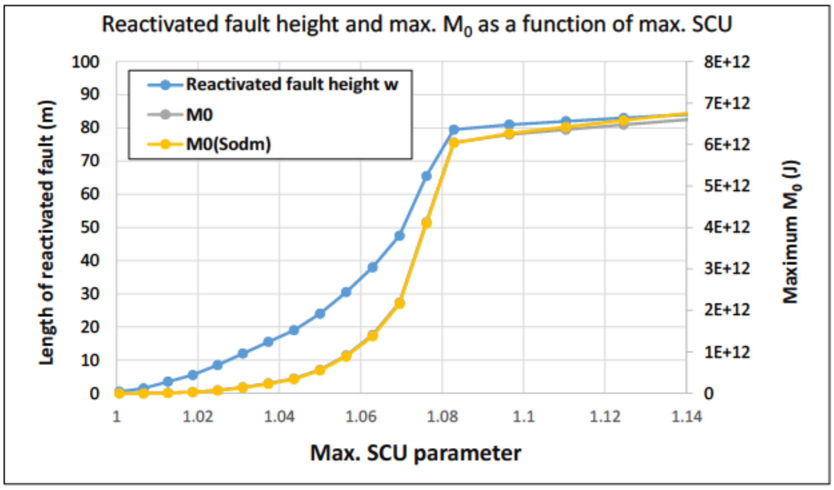

Figure 5-6 Reactivated fault height w and maximum seismic moment M_0 as a function of maximum SCU: zoom-in of figure 5-5 for SCU between 1 and 1.14, after three years of injection and injector-fault distance of 100 m.

Once the two peaks and valley in between of the SCU-profile all are in the range of SCU $\geq$ 1, further increase in the maximum SCU results in a modest increase of the reactivated fault height (Figures 5-5 and 5-6). In this particular example, this boundary is located at maximum SCU = 1.08. Not surprisingly, the seismic moment M_0 follows the reactivated fault height w. This is entirely in line with equation (5.1).

Finally, as Figure 5-5 shows, for high values of the maximum SCU-parameter, the curve labeled “M_0” bends down whereas the curve labeled “M_0(Sodm)” keeps increasing. The reason for the curve “M_0” bending down is that very high values of SCU result from a lower effective normal stress on the fault as a result of cooling. From Figure 5-3 it follows that this results in a lower relaxation stress $\Delta\sigma$. As can be also seen, the maximum difference between the “M_0”-curve and “M_0(Sodm)”-curve is equal to about a factor 2. In terms of magnitude this amounts to a difference of about $^{10}\log(2) \approx 0.3$.

Figure 5-7 shows the maximum magnitude M_w as computed using (5.2) as a function of maximum SCU. As a result of the logarithmic character of M_w, the two “regimes” (i.e. SCU<1.08, SCU$\geq$1.08) in the dependency of M_w on maximum SCU are even more pronounced than in Figures 5-5 and 5-6.

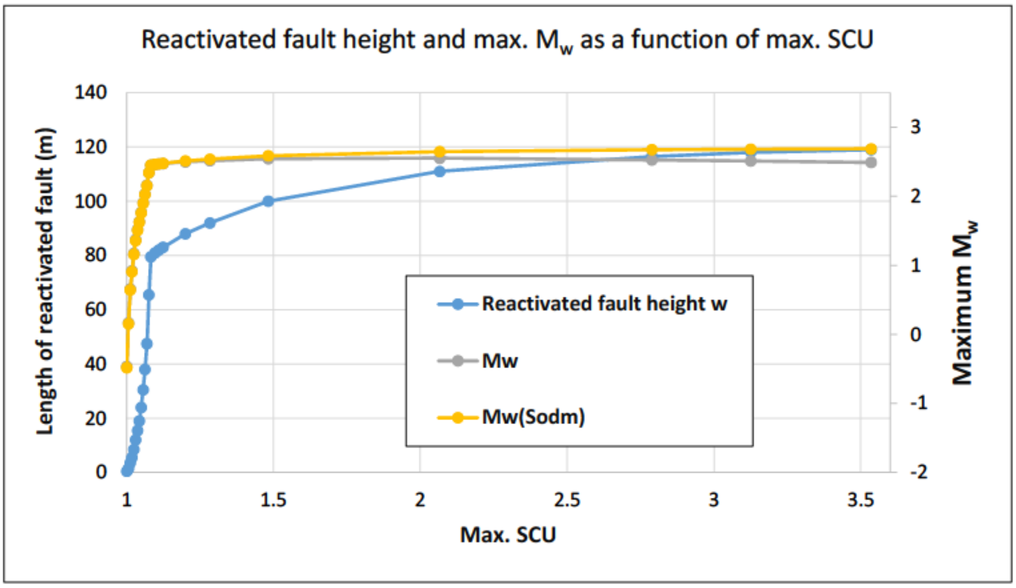

Figure 5-7 Reactivated fault height w and maximum magnitude M_w as a function of maximum SCU, after three years of injection and injector-fault distance of 100 m.

With the use of Figure 5-7 a distribution of maximum possible magnitude M_w is generated. The maximum magnitude M_w is ~2.5.

5.5.2. Fault-injector distance 250 m

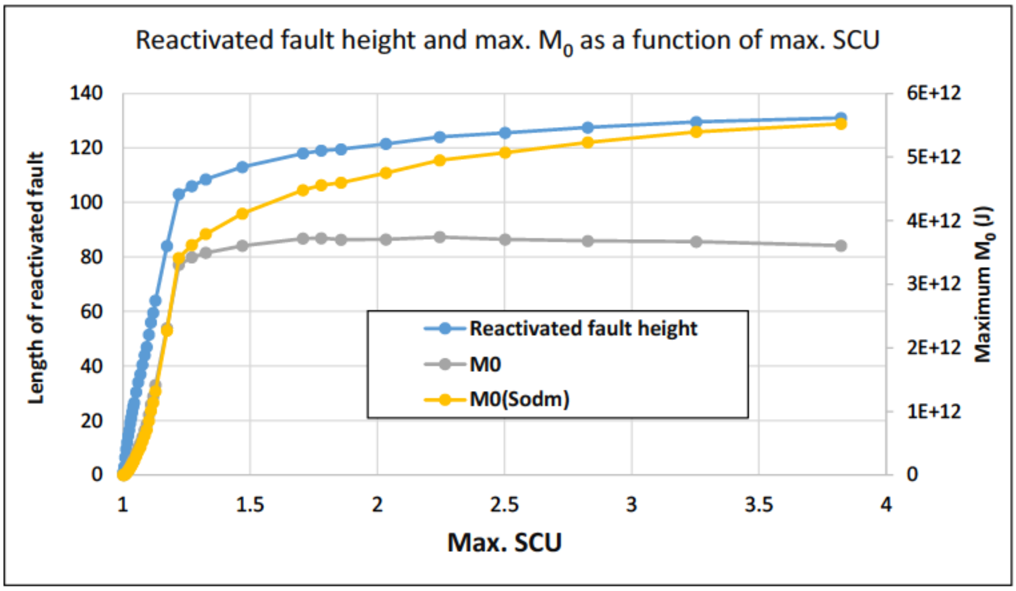

Figure 5-8 Reactivated fault height w and maximum seismic moment M_0 as a function of maximum SCU, after three years of injection and injector-fault distance of 250 m.

Figure 5-8 shows the reactivated fault height w and seismic moment M_0 as a function of maximum SCU. Again it can be seen that initially (for SCU $\leq$ 1.22), the reactivated fault height increases rapidly as a function of maximum SCU. A zoom-in of the results of Figure 5-8 on maximum SCU-range between 1 and 1.3 is depicted in Figure 5-9, clearly illustrating this point.

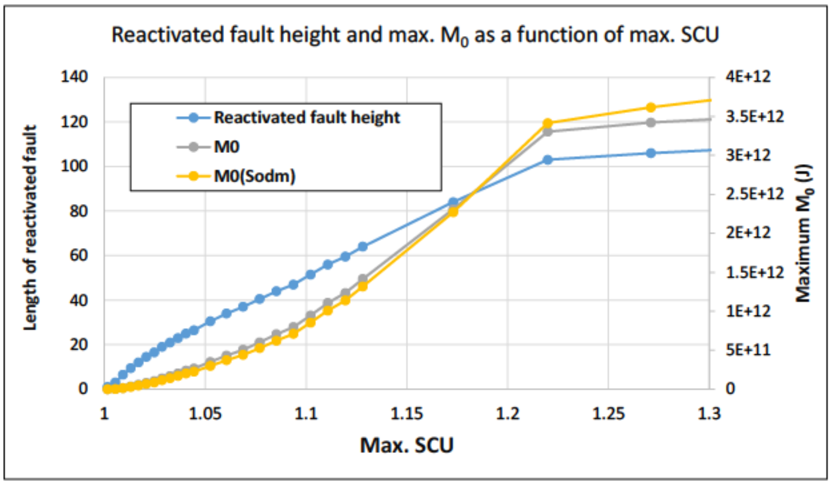

Figure 5-9 Reactivated fault length and maximum seismic moment M_0 as a function of maximum SCU: zoom-in of figure 5-8 for SCU between 1 and 1.3, after three years of injection and injector-fault distance of 250 m.

As before, in Figures 5-8 and 5-9, two curves for M_0 are indicated. In this case, the maximum difference between the "M_0"-curve and "M_0(Sodm)"-curve is equal to about a factor 1.5. In terms of magnitude this amounts to a difference of about $^{10}\log(1.5) \approx 0.2$.

Figure 5-10 shows the maximum magnitude M_w as computed using (5.2) as a function of maximum SCU.

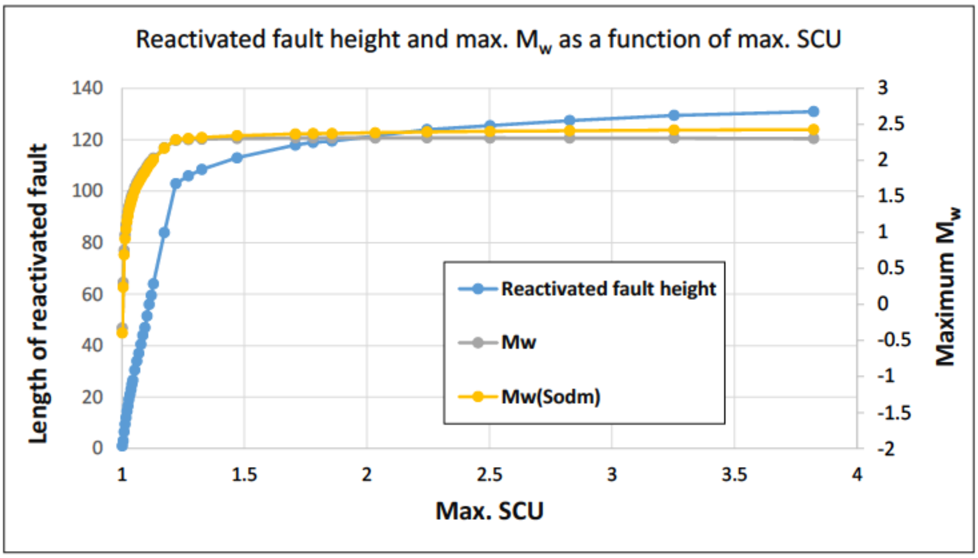

Figure 5-10 Reactivated fault height w and maximum magnitude M_w as a function of maximum SCU, after three years of injection and injector-fault distance of 250 m.

With the use of Figure 5-10 a distribution of maximum possible magnitude M_w is generated. The maximum possible magnitude M_w is ~2.3.

5.5.3. Fault-injector distance 400 m

For a fault at 400 m from the injector and after three years of injection, the entire fault is still at reservoir temperature. For such a situation it is difficult to use the SodM method for the computation of M_0. Because of this, and because the situation is very close to a pre-cooling (pre-injection) situation, no attempt was undertaken to estimate M_0.

5.6 Temperature profile and deterministic analysis after 35 years of injection

The computed temperature profile away from the injector after 35 years of injection is presented in Figure 5-11. As can be seen, in this case the cold front has (almost) entirely crossed the fault, irrespective of its distance to the injector (100m, 250 m or 400 m). Consequently, no significant differences are expected for these three different cases.

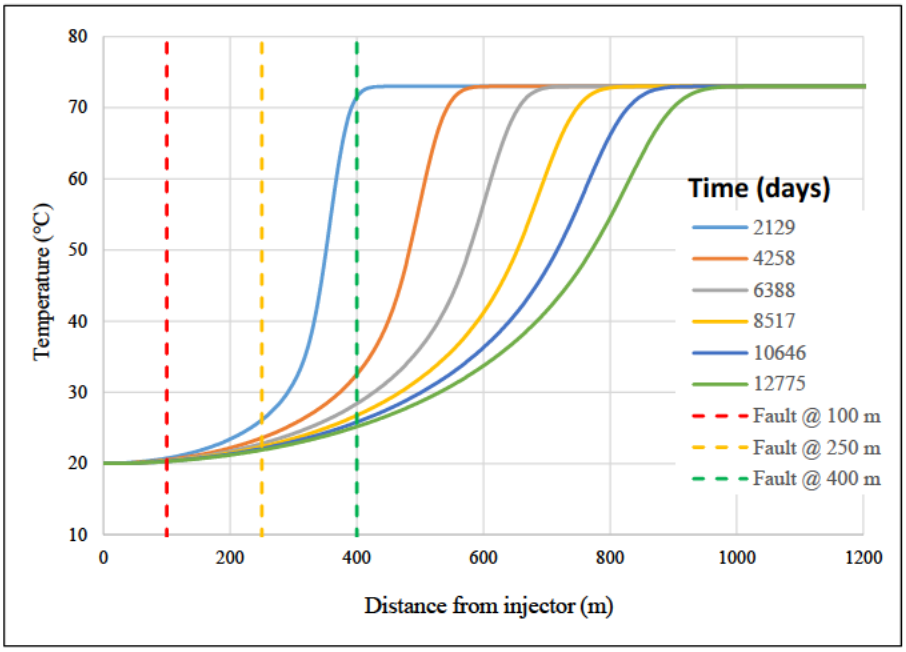

Figure 5-11 Temperature profile in the reservoir away from the injector after 35 years of injection.

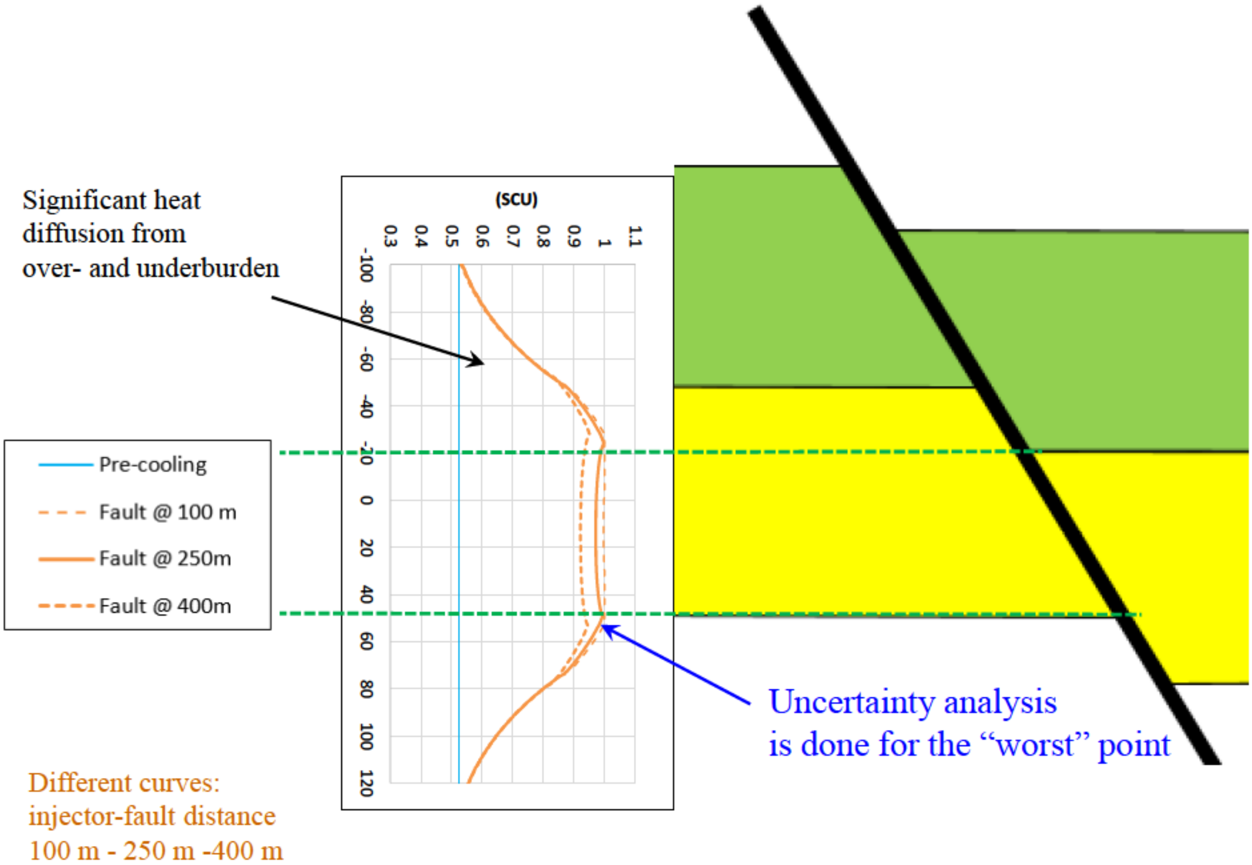

Figure 5-12 Computed SCU along the fault after 35 years of injection. The "worst point" is addressed in a Monte-Carlo simulation. The three different curves indicate the SCU-profiles for a fault at 100 m – 250 m – 400 m.

The computed SCU-profiles along the fault after 35 years of injection are shown in Figure 5-. As expected, the SCU profiles for the three different cases show only minor differences, in line with the results of Figure 5-11.

5.7 Uncertainty analysis and maximum M_w after 35 years of injection

5.7.1. Fault-injector distance 100 m

The maximum fault reactivation energy is calculated as explained in section 5.4 above.

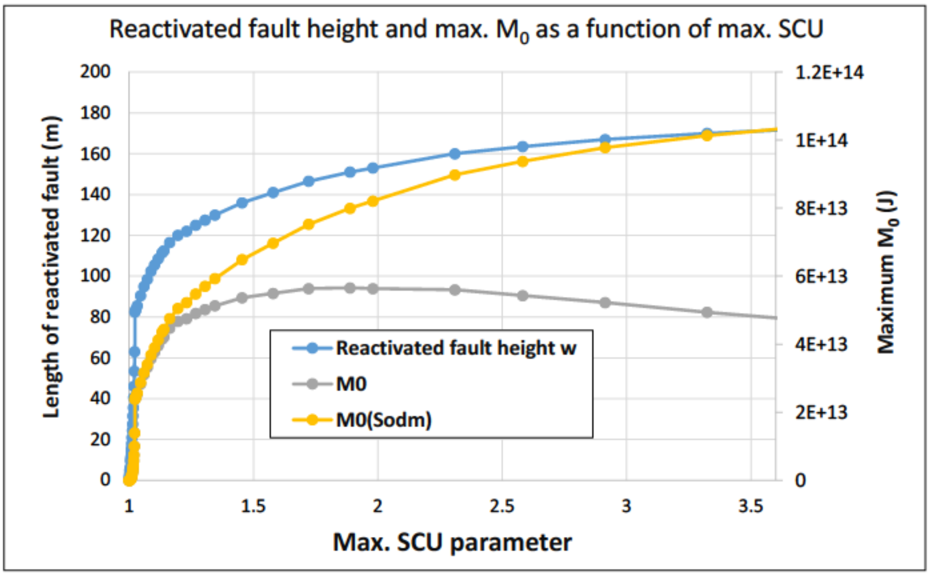

Figure 5-13 Reactivated fault height w and maximum seismic moment M_0 as a function of maximum SCU, after 35 years of injection and injector-fault distance of 100 m.

Figure 5-13 shows the reactivated fault height w and seismic moment M_0 as a function of maximum SCU. As before, it can be seen that initially (for SCU $\leq$ 1.025), the reactivated fault height increases rapidly as a function of maximum SCU. A zoom-in of the results of Figure 5-13 on maximum SCU-range between 1 and 1.14 is depicted in Figure 5-14, clearly illustrating this point.

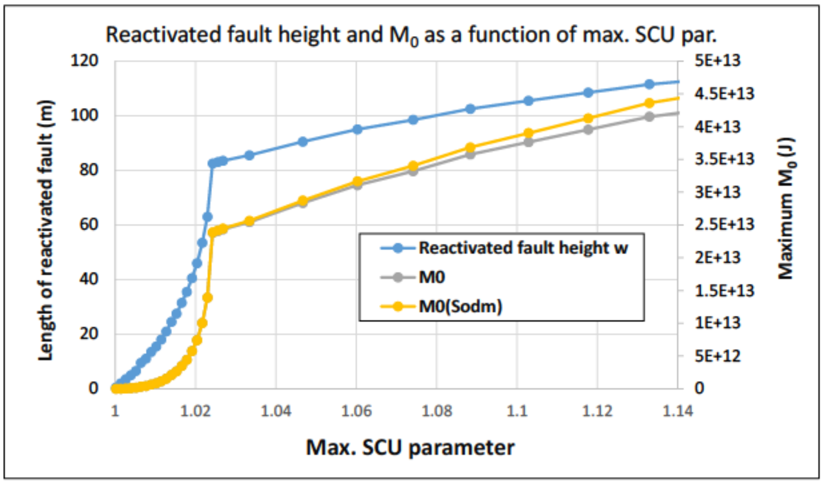

Figure 5-14 Reactivated fault length and maximum seismic moment M_0 as a function of maximum SCU: zoom-in of figure 5-13 for SCU between 1 and 1.14, after 35 years of injection and injector-fault distance of 100 m.

As before, in Figures 5-13 and 5-14, two curves for M_0 are indicated. The maximum difference between the "M_0"-curve and "M_0(Sodm)"-curve is equal to about a factor 2. In terms of magnitude this amounts to a difference of about $^{10}\log(2.0) \approx 0.3$.

Figure 5-15 shows the maximum magnitude M_w as computed using (5.2) as a function of maximum SCU.

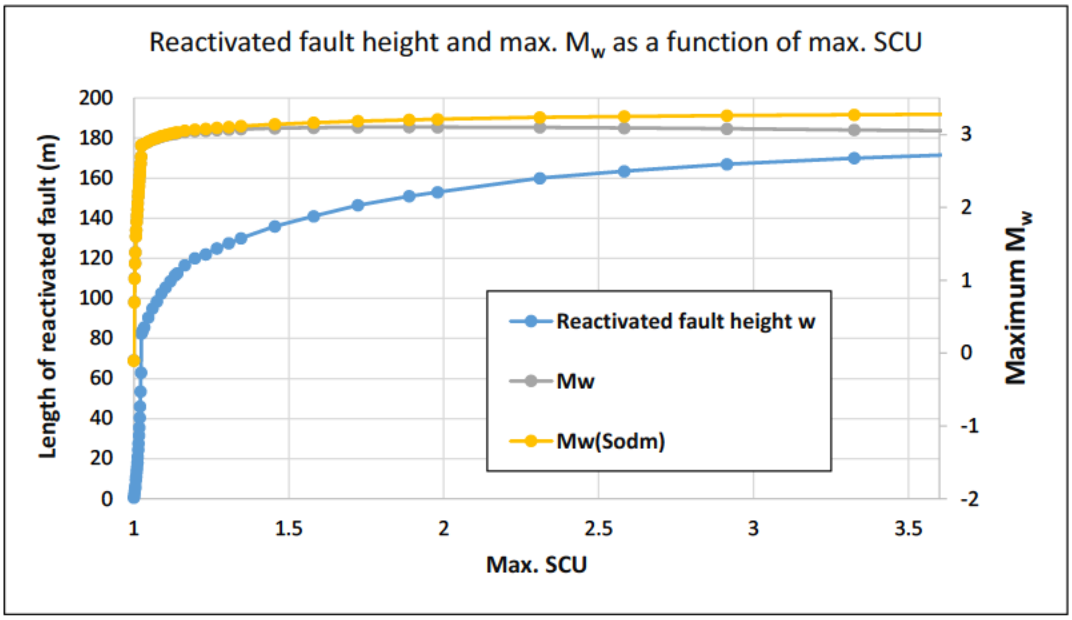

Figure 5-15 Reactivated fault height w and maximum magnitude M_w as a function of maximum SCU, after 35 years of injection and injector-fault distance of 100 m.

With the use of Figure 5-15 a distribution of maximum possible magnitude M_w is generated. The maximum possible magnitude M_w is ~3.1. The difference between this value and the value of maximum M_w ~ 2.5 for 3 years injection can be entirely explained by the fact that both the height *w* (through thermal diffusion into cap- and baserock) and the front length *L* (through cumulative injection) have significantly increase between 3 years and 35 years.

5.7.2. Fault-injector distance 250 m

The maximum fault reactivation energy is calculated as explained in section 5.4 above.

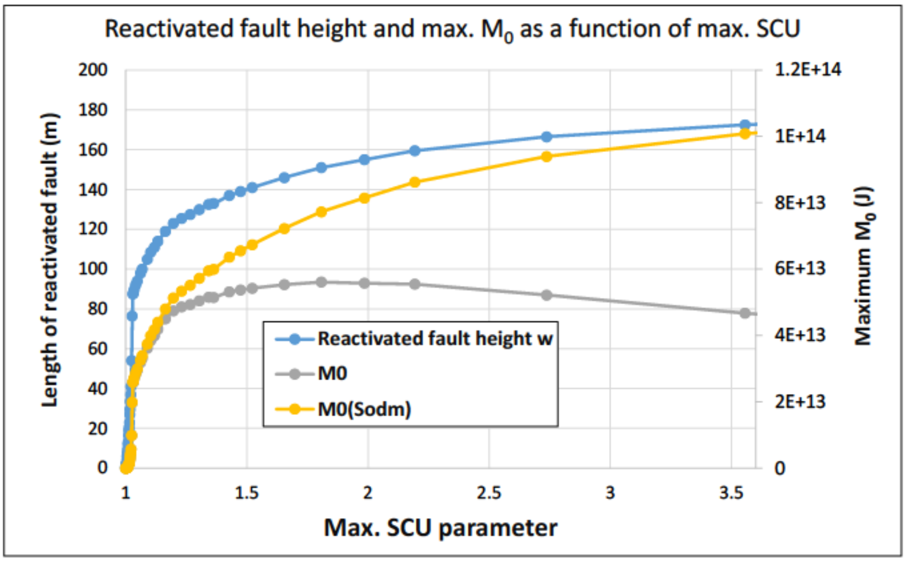

Figure 5-16 Reactivated fault height w and maximum seismic moment M_0 as a function of maximum SCU, after 35 years of injection and injector-fault distance of 250 m.

Figure 5-16 shows the reactivated fault height w and seismic moment M_0 as a function of maximum SCU. As before, it can be seen that initially (for SCU $\leq$ 1.03), the reactivated fault height increases rapidly as a function of maximum SCU. A zoom-in of the results of Figure 5-16 on maximum SCU-range between 1 and 1.14 is depicted in Figure 5-17, clearly illustrating this point.

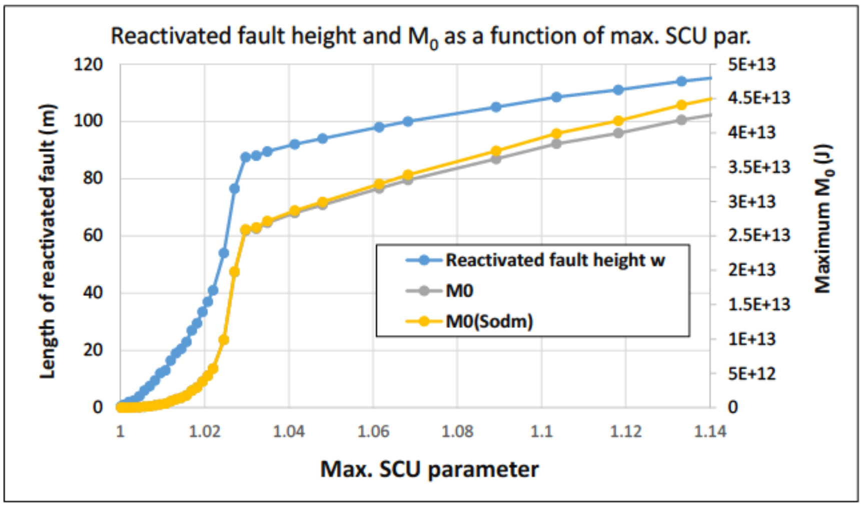

Figure 5-17 Reactivated fault length and maximum seismic moment M_0 as a function of maximum SCU: zoom-in of figure 5-13 for SCU between 1 and 1.14, after 35 years of injection and injector-fault distance of 250 m.

As before, in Figures 5-16 and 5-17, two curves for M_0 are indicated. Also in this case, the maximum difference between the "M_0"-curve and "M_0(Sodm)"-curve is equal to about a factor 2. In terms of magnitude this amounts to a difference of about $^{10}\log(2.0) \approx 0.3$.

Figure 5-18 shows the maximum magnitude M_w as computed using (5.2) as a function of maximum SCU.

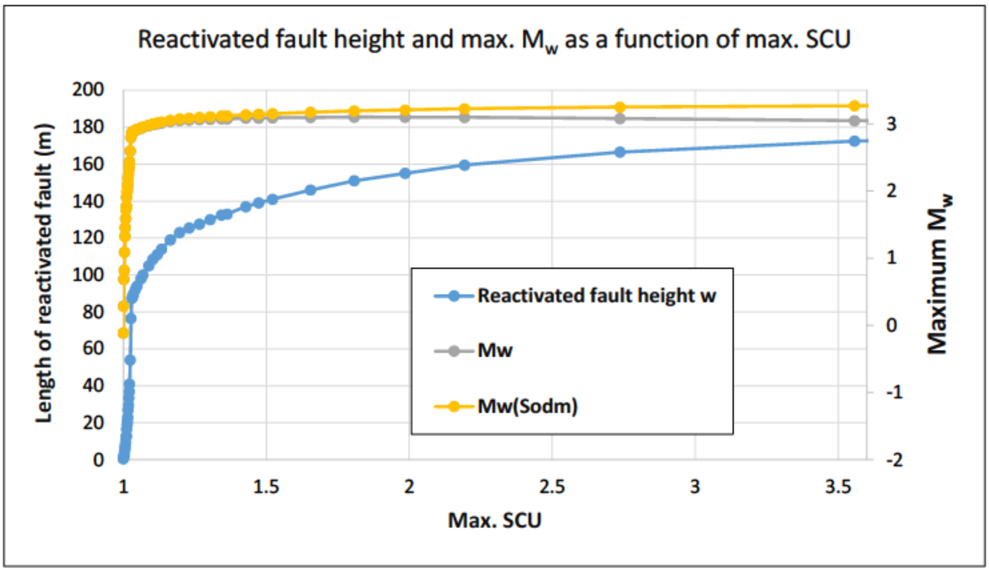

Figure 5-18 Reactivated fault height w and maximum magnitude M_w as a function of maximum SCU, after 35 years of injection and injector-fault distance of 250 m.

With the use of Figure 5-18 a distribution of maximum possible magnitude M_w is generated. The maximum possible magnitude M_w is ~3.1. This is very similar to the case of injector-fault distance 100 m, in line with expectations.

5.7.3. Fault-injector distance 400 m

The maximum fault reactivation energy is calculated as explained in section 5.4 above.

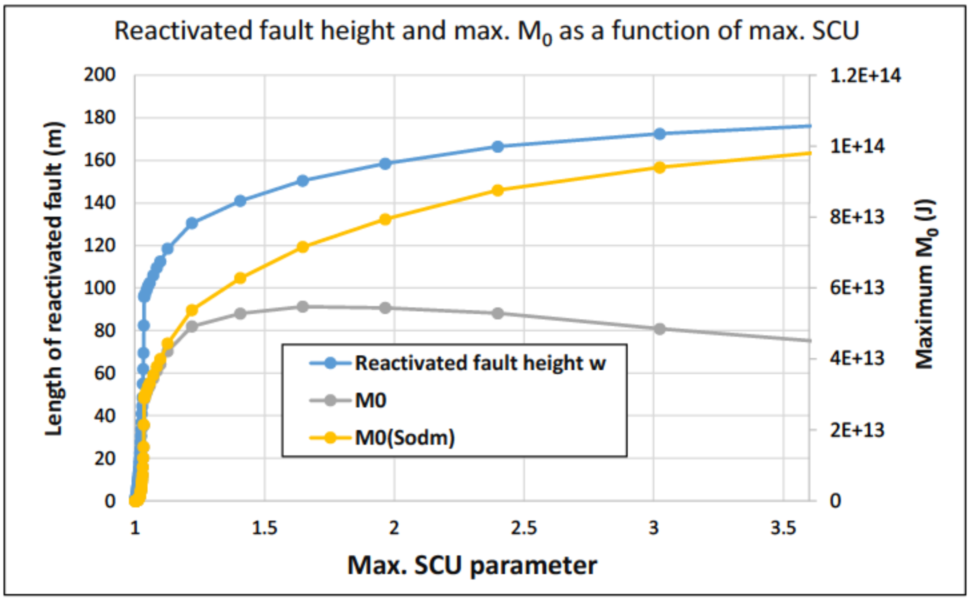

Figure 5-19 Reactivated fault height w and maximum seismic moment M_0 as a function of maximum SCU, after 35 years of injection and injector-fault distance of 400 m.

Figure 5-19 shows the reactivated fault height w and seismic moment M_0 as a function of maximum SCU. As before, it can be seen that initially (for SCU $\leq$ 1.035), the reactivated fault height increases rapidly as a function of maximum SCU. A zoom-in of the results of Figure 5-19 on maximum SCU-range between 1 and 1.14 is depicted in Figure 5-20, clearly illustrating this point.

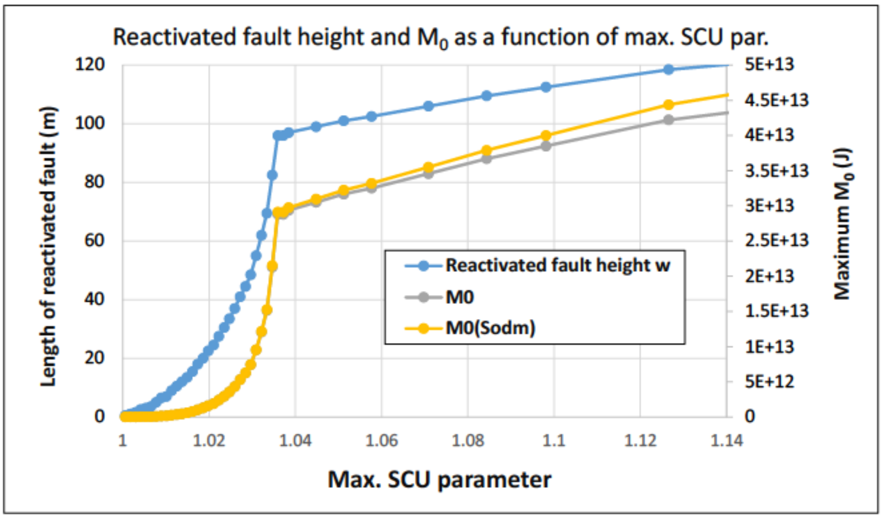

Figure 5-20 Reactivated fault length and maximum seismic moment M_0 as a function of maximum SCU: zoom-in of figure 5-19 for SCU between 1 and 1.14, after 35 years of injection and injector-fault distance of 400 m.

As before, in Figures 5-19 and 5-20, two curves for M_0 are indicated. Also in this case, the maximum difference between the "M_0"-curve and "M_0(Sodm)"-curve is equal to about a factor 2. In terms of magnitude this amounts to a difference of about $^{10}\log(2.0) \approx 0.3$.

Figure 5-21 shows the maximum magnitude M_w as computed using (5.2) as a function of maximum SCU.

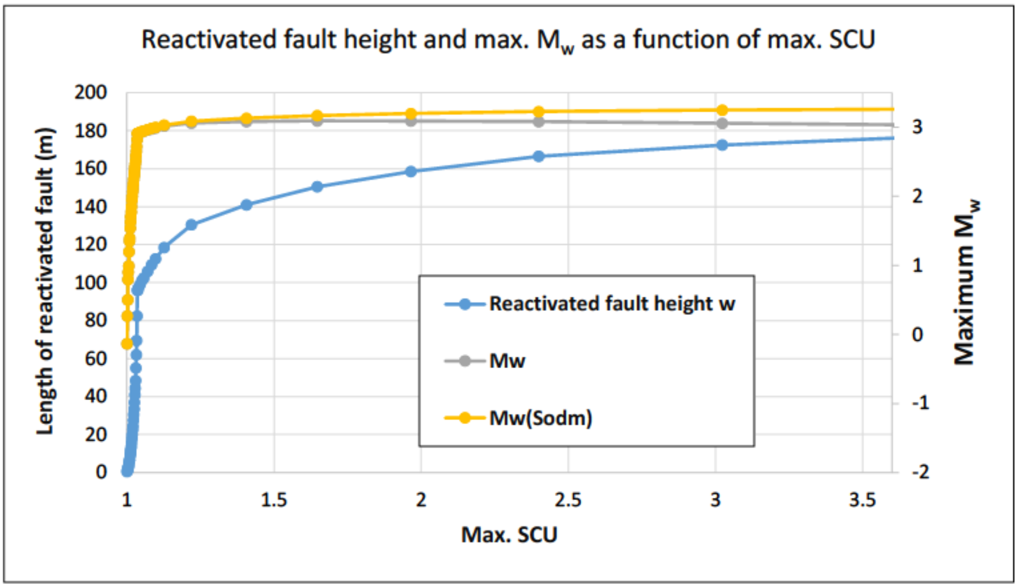

Figure 5-21 Reactivated fault height w and maximum magnitude M_w as a function of maximum SCU, after 35 years of injection and injector-fault distance of 400 m.

With the use of Figure 5-21 a distribution of maximum possible magnitude M_w is generated. The maximum possible magnitude M_w is ~3.1. This is very similar to the cases of injector-fault distance 100 m and 250 m, in line with expectations.

6 Conclusions

This report presents a level-2 SHA study for Geothermie Delft (GTD). The study has been carried out for the situation after 3 years of operation and after 35 years of operation of the doublet.

A conservative approach was applied for all cases in the sense that:

(1) It was assumed that the fault is non-sealing. As a result, a maximum size of the cooled zones on either side of the fault was achieved in the study, thus leading to minimal scope for arching by adjacent uncooled zones.
(2) It was assumed that slip occurs at once for the entire area of the fault where SCU ≥ 1
(3) An upper bound to the maximum possible magnitude M_w was estimated based on the assumption that the formation rock around the fault behaves in an elastic-brittle manner in response to cooling-induced stress disturbances, as a result of which all fault reactivation energy is released at once.
(4) No difference in horizontal in-situ stress between reservoir and cap-/baserock was assumed.
(5) The same fault strength is assumed over the entire reservoir and over cap-/baserocks.

The results show that for the situation after 3 years of operation, the realistically strongest possible seismic tremor as a result of fault slip clearly depends on the distance between the injector and the nearest fault. For a distance of 100 m, the maximum possible magnitude M_w is equal to 2.5. For a distance of 250 m this is equal to 2.3, whilst for a distance of 400 m, fault stability has hardly changed with respect to the pre-cooling (pre-injection) situation.

For the situation after 35 years of operation, the realistically strongest possible seismic tremor as a result of fault slip hardly depends on the distance between the injector and the nearest fault. In this situation the maximum possible magnitude M_w is equal to 3.1.

Until now, no seismic events or small earthquakes have been reported as a result of geothermal operations in The Netherlands. In the future, if seismic sensors would detect seismic activity resulting from geothermal operations, the models can be calibrated and predictions could be updated.

7 References

Buijze, L., van den Bogert, P. A. J., Wassing, B. B. T., Orlic, B., & ten Veen, J. (2017). Fault reactivation mechanisms and dynamic rupture modelling of depletion-induced seismic events in a Rotliegend gas reservoir. *Netherlands Journal of Geosciences*, *96*(5), s131–s148. https://doi.org/10.1017/njg.2017.27

de Jager, J., Doyle, M. A., Grantham, P. J., & Mabillard, J. E. (1996). Hydrocarbon habitat of the West Netherlands Basin. In H. E. Rondeel, D. A. J. Batjes, & W. H. Nieuwenhuijs (Eds.), *Geology of Gas and Oil under the Netherlands* (pp. 191–209). Springer Netherlands. https://doi.org/10.1007/978-94-009-0121-6_17

Duin, E. J. T., Doornenbal, J. C., Rijkers, R. H. B., Verbeek, J. W., & Wong, Th. E. (2006). Subsurface structure of the Netherlands—Results of recent onshore and offshore mapping. *Netherlands Journal of Geosciences - Geologie En Mijnbouw*, *85*(4), 245–276. https://doi.org/10.1017/S0016774600023064

Hunfeld, L. B., Niemeijer, A. R., & Spiers, C. J. (2017). Frictional Properties of Simulated Fault Gouges from the Seismogenic Groningen Gas Field Under In Situ *P* - *T* -Chemical Conditions: Friction of Groningen fault gouges. *Journal of Geophysical Research: Solid Earth*, *122*(11), 8969–8989. https://doi.org/10.1002/2017JB014876

Koning, E. J. L. (1988). *Waterflooding under fracturing conditions*. http://citeseerx.ist.psu.edu/viewdoc/download?doi=10.1.1.913.17&rep=rep1&type=pdf

Perkins, T. K., & Gonzalez, J. A. (1985). The Effect of Thermoelastic Stresses on Injection Well Fracturing. *Society of Petroleum Engineers Journal*, *25*(01), 78–88. https://doi.org/10.2118/11332-PA

Poessé, J. W., & van den Hoek, P. (2020). Semi-Quantitative Assessment of Seismic Hazard in Geothermal Reservoirs. SPE-200544*, presented at the SPE Europec featured at the 82nd EAGE Conference and Exhibition held virtually, 1-3 December, 2020*. D011S004R003. https://doi.org/10.2118/200544-MS

Q-CON/IF technology. (2016). *Defining the Framework for Seismic Hazard Assessment in Geothermal Projects V0.1*. https://www.kasalsenergiebron.nl/content/user_upload/Kennisagenda_-_Defining_framework_for_Seismic_Hazard_Assessment_in_Geothermal_Projects_-_Technical_Report_-_161005.pdf

Samuelson, J., & Spiers, C. J. (2012). Fault friction and slip stability not affected by Co2 storage: Evidence from short-term laboratory experiments on North Sea reservoir sandstones and caprocks. *International Journal of Greenhouse Gas Control*, *11*, S78–S90. https://doi.org/10.1016/j.ijggc.2012.09.018

Santarelli, F. J., Havmoller, O., & Naumann, M. (2008). Geomechanical Aspects of 15 Years Water Injection on a Field Complex: An Analysis of the Past to Plan the Future. *All Days*, SPE-112944-MS. https://doi.org/10.2118/112944-MS

Staatstoezicht op de Mijnen (2016). Methodiek voor risicoanalyse omtrent geïnduceerde bevingen door gaswinning. Tijdelijke leidraad voor adressering mbb. 24.1.p, versie 1.2

Stevens, D. G., Murray, L. R., & Shah, P. C. (2000). Predicting Multiple Thermal Fractures in Horizontal Injection Wells; Coupling of a Wellbore and a Reservoir Simulator. *All Days*, SPE-59354-MS. https://doi.org/10.2118/59354-MS

Svendsen, A. P., Wright, M. S., Clifford, P. J., & Berry, P. J. (1991). Thermally Induced Fracturing off Ula Water Injectors. *SPE Production Engineering*, *6*(04), 384–390. https://doi.org/10.2118/20898-PA

TNO. (2014). *DoubletCalc 1.4 manual*. TNO. https://www.nlog.nl/sites/default/files/6ab98fc3-1ca1-4bbe-b0a2-c5a9658a3597_doubletcalc%20v143%20manual.pdf

van den Bogert, P. (2015). *Impact of various modelling options on the onset of fault slip and the fault slip reponse using 2-dimensional Finite- Element modelling.* https://www.researchgate.net/publication/348785769_Impact_of_various_modelling_options_on_the_onset_of_fault_slip_and_the_fault_slip_reponse_using_2-dimensional_Finite-_Element_modelling van den Hoek, P. J., & Poessé, J. W. (2021). Assessment of Seismic Risk in Geothermal and Hydrocarbon Reservoirs Using an Exact Analytical Solution of Stress Change. SPE-205122, *presented at the SPE Europec featured at the 83rd EAGE Conference and Exhibition held in Amsterdam, The Netherlands, 18-20 October*. D031S007R002. https://doi.org/10.2118/205122-MS

Verweij, J. M., Simmelink, H. J., Underschultz, J., & Witmans, N. (2012). Pressure and fluid dynamic characterisation of the Dutch subsurface. *Netherlands Journal of Geosciences - Geologie En Mijnbouw*, *91*(4), 465–490. https://doi.org/10.1017/S0016774600000342